2005

ION MOTION AND AN OPTIMIZATION OF TANDEM MASS SPECTROMETRY

John Edward Spencer
University of Kentucky, jespen2@uky.edu

ABSTRACT OF THESIS

ION MOTION AND AN OPTIMIZATION OF TANDEM MASS SPECTROMETRY

Quadrupole ion trap(QIT) mass spectrometry has become one of the most widely used tools in the analysis of the structure of small molecules. The motion of the ions stored in the quadrupole ion trap is extremely important. This ion motion within the quadrupole ion trap is controlled by several factors including the m/z ratio and the collisional cross section of the ion. Investigation of ion motion within the QIT has the potential to elucidate a new way to separate ions based on these factors. DC tomography experiments allow for the trajectory of the ion motion to be measured without modifications to the ion trap. The ability to use DC tomography for separation of isomeric ions on a commercial GC/MS system was investigated.

Investigation of the mass range within the ion trap is necessary for the analysis of a wide range of molecules. The ability of the quadrupole ion trap to perform MS/MS analyses can provide insight into the structural information of many compounds. However, there exists a low mass cut-off (LMC) within the quadrupole ion trap and thus information about the low m/z fragments from a parent ion is lost. Schwartz and co-workers presented a new technique labeled pulsed q dissociation (PQD) at the 53rd Annual ASMS Conference in San Antonio TX in 2005. PQD eliminates the LMC by performing CID at a q_z of 0.4 but, then immediately lowering the q level before the mass scan in a linear ion trap. By operating the quadrupole ion trap in this same manner, low m/z product ions can be detected. This technique and elucidation of the energetic process contained within PQD were explored further using a modified commercial quadrupole ion trap and the results discussed in this work.

KEYWORDS: Mass Spectrometry, Quadrupole Ion Trap, Collision Induced Dissociation, Tandem Mass Spectrometry, Ion Mobility

_____

_____

ION MOTION AND AN OPTIMIZATION OF TANDEM MASS SPECTROMETRY

By

John Edward Spencer

_____
Director of Thesis

_____
Co-Director of Thesis

_____
Co-Director of Thesis

_____
Director of Graduate Studies

_____

RULES FOR THE USE OF THESES

Unpublished theses submitted for the Master's degree and deposited in the University of Kentucky Library are as a rule open for inspection, but are to be used only with due regard to the rights of the authors. Bibliographical references may be noted, but quotations or summaries of parts may be published only with the permission of the author, and with the usual scholarly acknowledgments.

Extensive copying or publication of the thesis in whole or in part also requires the consent of the Dean of the Graduate School of the University of Kentucky.

A library that borrows this thesis for use by its patrons is expected to secure the signature of each user.

Name	Date

THESIS

John Edward Spencer

The Graduate School

University of Kentucky

2005

ION MOTION AND AN OPTIMIZATION OF TANDEM MASS SPECTROMETRY

THESIS

A thesis submitted in partial fulfillment of the
requirements for the degree of Master of Science in the
College of Arts and Sciences
at the University of Kentucky

By

John Edward Spencer

Lexington, Kentucky

Director: Dr. Bert C. Lynn, Professor of Chemistry

Lexington, Kentucky

2005

MASTER’S THESIS RELEASE

I authorize the University of Kentucky
Libraries to reproduce this thesis in
whole or in part for purposes of research.

Signed:_____
Date:_____

ACKNOWLEDGMENTS

The following thesis, while an individual work, benefited from the insights and direction of several people. First, my Thesis Chair, Dr. Bert C. Lynn, exemplifies the high quality scholarship to which I aspire. Next, I wish to thank the complete Thesis Committee: Dr. Bert C. Lynn, Dr. Mark A. Lovell, and Dr. Robert A. Lodder. Each individual provided insights that guided and challenged my thinking, substantially improving the finished product. I would also like to thank Dr. Jack Goodman for all of his technical and instrumental assistance without which research would be hard to do. In addition to the technical and instrumental assistance above, I received equally important assistance from family and friends.

TABLE OF CONTENTS

LIST OF TABLES

LIST OF FIGURES

CHAPTER 1

Quadrupole Ion Trap Theory

Quadrupole ion trap(QIT) mass spectrometry(MS) is an important analytical tool that can be used to gain information that includes the elemental composition of matter and the structures of molecules. Qualitative and quantitative information on complex mixtures can also be obtained using mass spectrometry. Detailed information on the structure and composition of complex mixtures, as well as isotopic ratios of atoms can be acquired with a QITMS.[1]

The physical characteristics of a QIT include a donut shaped ring electrode bounded by two end cap electrodes. All of the electrode elements contain a hyperbolic cross-section as shown in Figure 1.1.[1]

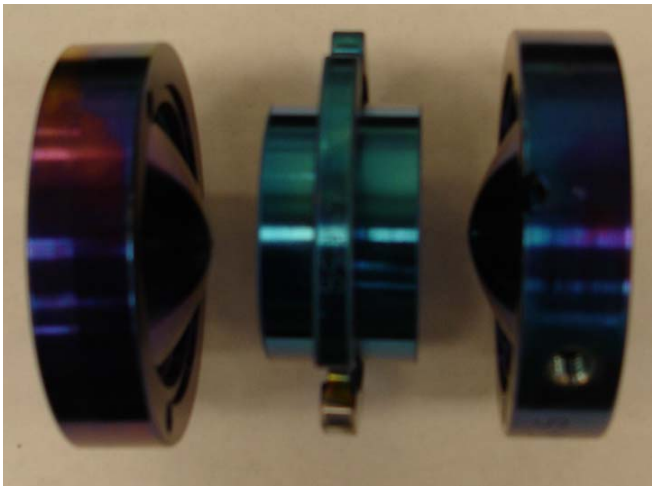

Figure 1.1. Physical characteristics of the quadrupole ion trap.

Components of a commercial QIT mass spectrometer are shown in Figure 1.2 and consist of an inlet system for the introduction of analyte, an ion source for ionization of the analyte, a mass analyzer for the separation or storage of ions, and a detector for the detection of ions.

A common inlet system for sample introduction into the QIT is the gas chromatograph (GC). GC consists of both a stationary and mobile phases. The stationary phase typically consists of fused silica coated with (5%-phenyl)-methylpolysiloxane, while the mobile phase is a low molecular weight inert gas such as

helium.[1] Gas chromatography separates organic compounds based on their unique vapor pressures and interaction with the solid phase support on the column.

From the column of the GC, compounds then enter the MS. Another important physical characteristic of the QIT is the helium present which acts as a bath gas. Throughout the operation of the QIT, molecules are constantly being cooled in kinetic energy to the center of the trap by colliding with helium atoms.[2] The effect of this bath gas depends on the pressure and temperature of the helium within the trap. When the pressure of helium is 1 mtorr, molecules collide with helium atoms at a rate of 30 per millisecond.

Modern commercial QIT's have three main modes of operation: ionization of molecules, storage of ions based on the mass to charge ratio(m/z), and detection of ions.[2]

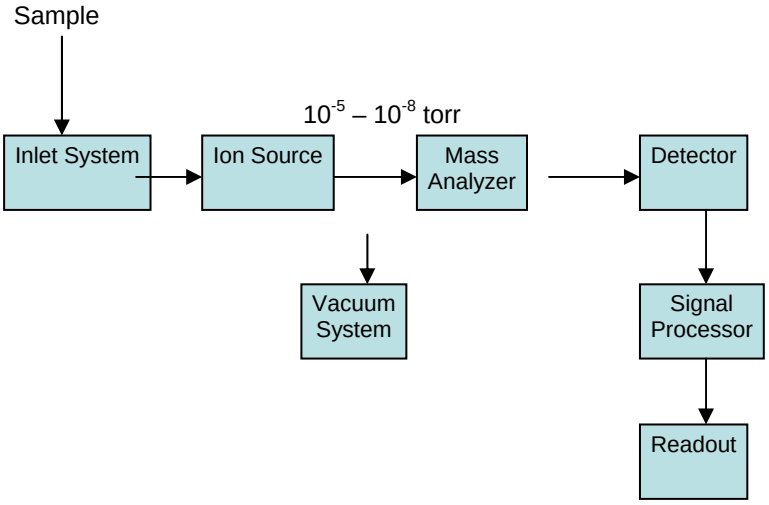

Figure 1.2. Components of a Mass Spectrometer.

Molecules that enter the trap are ionized by electron impact ionization (EI). EI sources employ a beam of 70 eV electrons directed toward the molecules. The electron beam is produced by a heated tungsten or rhenium filament and propelled toward the center of the trap by an accelerating potential shown in Figure 1.3.[1] Electron impact ionization is a very inefficient process as only one in a million molecules undergo the main reaction:[1]

$$M + e^- \rightarrow M^{*+} + 2e^- \quad (1)$$

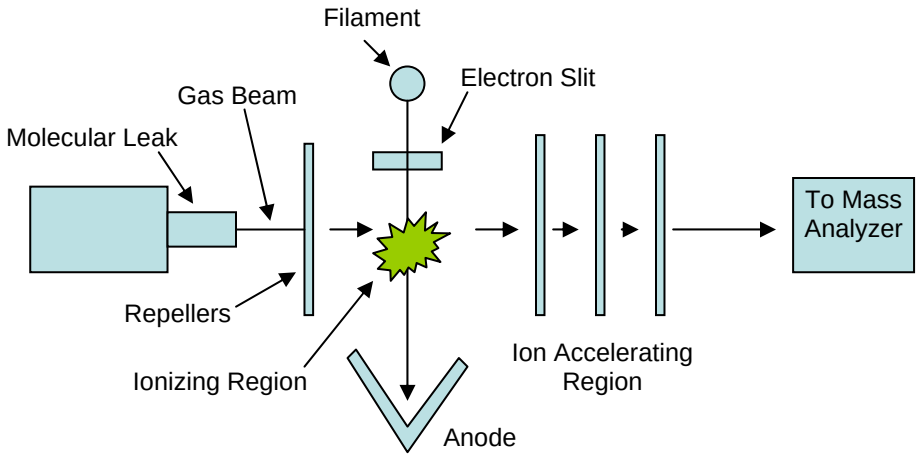

Figure 1.3. Electron impact ionization source.

The main reaction shown in Equation 1 occurs as electrons from the electron beam move past the molecule leading to a resonant interaction with an electron in the outermost energy level of the molecule. The electron from the outer most energy level of the molecule is removed forming a radical cation in a highly excited rotational and vibrational state shown in Figure 1.4.[1]

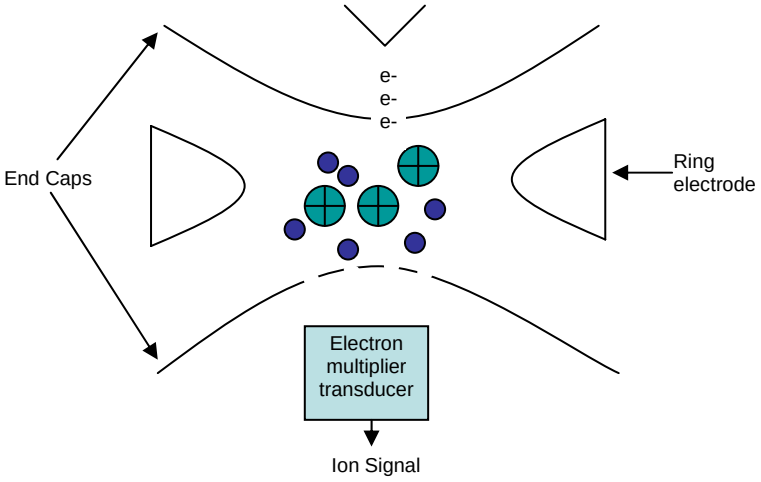

Figure 1.4. Quadrupole ion trap operation.

Since the radical cation is left in a highly excited rotational and vibrational state, the radical cation must fragment or rearrange in order to form energetically stable product ions. Should the radical cation be stable enough and later detected, then it is termed the

molecular ion. Fragmentation leaves two species, a neutral molecule and a positive ion. Since internal conversion processes in ions can occur in less than 10^{-7}s and unimolecular fragmentation may take up to 10^{-5} s, there exist many possibilities of fragmentation pathways as shown in Table 1.1.[1]

Fragmentation Pathways of Radical Cation from Electron Impact Ionization							
Molecular Ion Formation			$ABCD + e^-$	→	$ABCD^{\bullet+} + 2e^-$		
Fragmentation			$ABCD^{\bullet+}$	→	$A^+ + BCD^\bullet$		
				→	$A^\bullet + BCD^+$	→	$BC^+ + D$
				→	$CD^\bullet + AB^+$	→	$B + A^+$
					$CD^\bullet + AB^+$	→	$A + B^+$
				→	$AB^\bullet + CD^+$	→	$D + C^+$
					$AB^\bullet + CD^+$	→	$C + D^+$
Rearrangement followed by fragmentation			$ABCD^{\bullet+}$	→	$ADBC^{\bullet+}$	→	$BC^\bullet + AD^+$
			$ABCD^{\bullet+}$	→	$ADBC^{\bullet+}$	→	$AD^\bullet + BC^+$
Collision followed by fragmentation			$ABCD^{\bullet+} + ABCD$	→	$(ABCD)^{\bullet 2+}$	→	$BCD^\bullet + ABCDA^+$

Table 1.1. Fragmentation pathways.

After ionization and subsequent fragmentation, the QIT stores ions by application of a radio frequency to the ring electrode and interaction of the the ions with the electric field formed within the trap.[2] When an electrical signal in the form of a radio frequency(RF) is applied to the ring electrode and the end cap electrodes are held at ground potential, a quadrupolar electrical field is formed as shown in Figure 1.5.[2] The dimensions of the stretched commercial QIT do not form an ideal quadrupolar geometry within the trap shown in Figure 1.5a, but have a stretched geometry in which the z axis is approximately two times greater than the r axis shown in Figure 1.5b. The stretching was necessary because the ideal geometry QIT had a problem with a "mass shift" in which ions were detected incorrectly at wrong m/z values.[2]

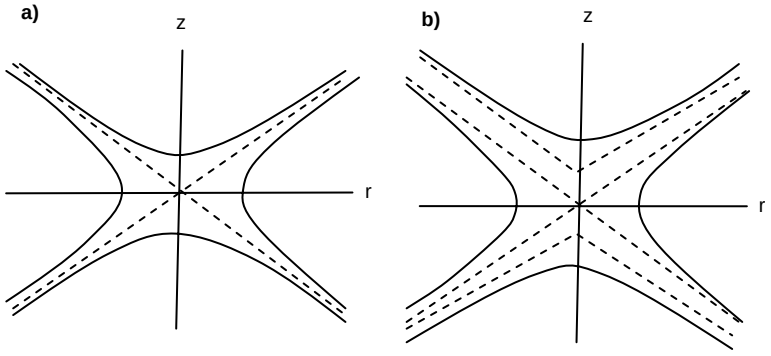

Figure 1.5. a) Pure Quadrupole field lines. b) Stretched geometry field lines.

Application of the RF to the ring electrode also gives rise to the so-called pseudo-potential well that is formed by the electric field of the quadrupolar field shown in Figure 1.6.[2] Both the depth of the pseudo-potential well and the kinetic energy of the ion increase as the RF amplitude are increased. Ions remain stable as long as the kinetic energy of the ions remains low enough not to eject them from the pseudo-potential well.

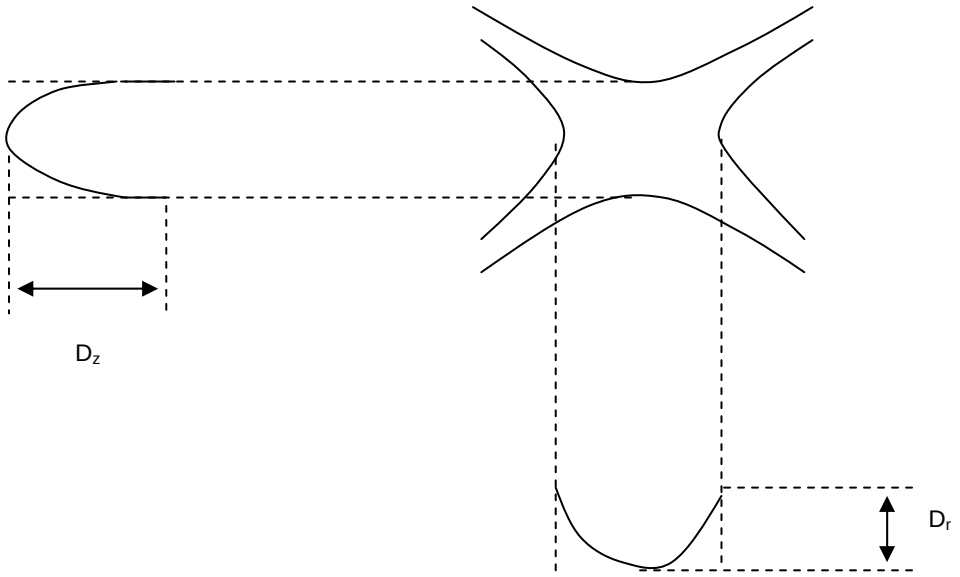

Figure 1.6. Pseudo-potential well.

Ions interact with the RF applied to the ring electrode and begin to orbit as the ions interact with the oscillatory motion of the electric field. The motion of the ions is important both axially and radially. Ions are stable within the ion trap so long as their trajectory in both the radial (r axis) and axial (z axis) directions conforms to the stable solutions of the Mathieu equation shown in Equation 2.[3]

$$a_z = -\frac{16eU}{m\left(r_0^2 + 2z_0^2\right)\Omega^2} \qquad q_z = -\frac{8eV}{m\left(r_0^2 + 2z_0^2\right)\Omega^2} \tag{2}$$

Where U is the DC potential (Volts) applied to the ring electrode, m is the molecular weight of the ion, *e* is the charge, r_0 is the radius of the trap, z_0 is the length of the trap, V is the RF amplitude (Volts) applied to the ring electrode, and Ω is the drive frequency (typically 1.1MHz).[2] A pictorial depiction of the boundary created by plotting the stable solutions to the Mathieu equations is shown in Figure 1.1.

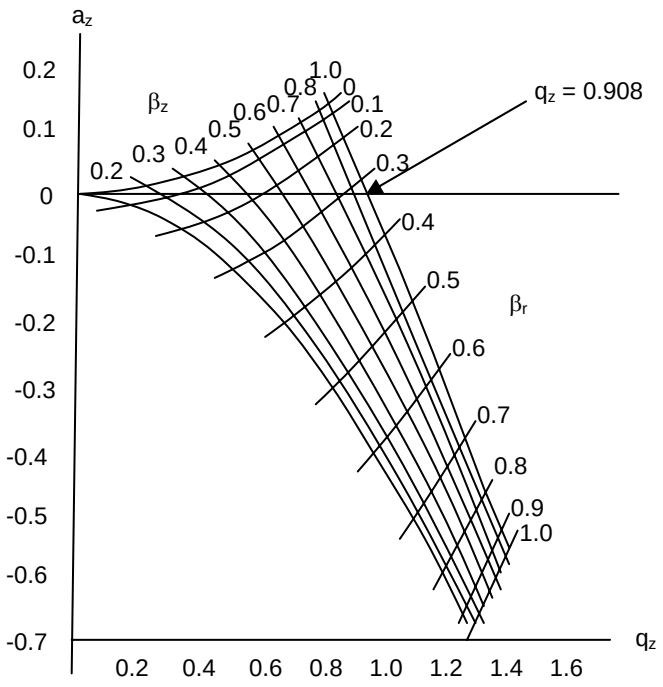

Figure 1.7. Mathieu stability diagram.

The motion of the ions within the trap is quite complex, so a more detailed explanation is necessary. The fundamental frequency at which the ion moves in all directions within the trap is called the fundamental secular frequency of the ion. There are two components that compose the fundamental secular frequency, ω_r and ω_z. These two components describe the secular frequency of the ion in both the radial, ω_r, and axial, ω_z, directions and can be described by the equation:[3]

$$\omega_{u,n} = (n + 0.5\beta_u)\Omega, \quad 0<n<\infty \tag{3}$$

$$\omega_{u,n} = -(n + 0.5\beta_u)\Omega, \quad -\infty<n<0 \tag{4}$$

Where $\beta_u \approx \sqrt{\left(a_u + \frac{q_u^2}{2}\right)}$ at low values of a and q (5)

and when considering only the axial component, β_z can be approximated to $\sqrt{\left(q_z^2/2\right)}$.(6)

The fundamental axial secular frequency is given by the equation:

$$\omega_z = \frac{\beta_z \Omega}{2} \tag{7}$$

From Equations 3-6, the radial(β_r) and axial(β_z) secular frequencies describe the actual motion of the ions, while from Equation 2 it can be determined that a and q merely relate m/z to voltage. However, the β_r and β_z are dependent on a_z and the q_z level at which the ion is stored. For the work in this paper, only the axial secular frequency will be considered further. The secular frequency can be described empirically by the motion of the ions in the x, y, and z directions within the trap. The trajectory of the ions within the trap forms a figure eight or what is termed a Lissajous curve shown in Figure 1.8.

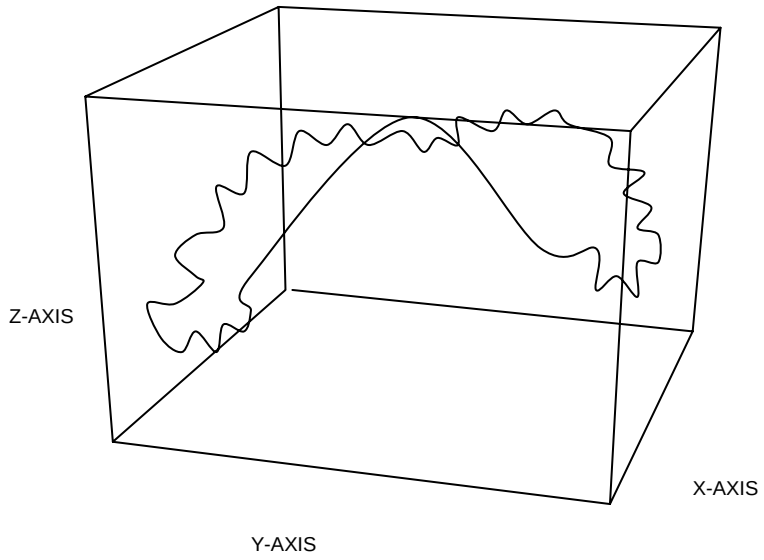

Figure 1.8 Lissajous curve of ion motion.

Equation 2 shows that an increase or decrease in the amplitude of the drive RF applied to the ring electrode increases or decreases the q_z level for a certain ion thus affecting the stability of the ion. As the RF amplitude is increased, the kinetic energy of the ions increases, and the trajectory of the ion becomes unstable within the trap. Ions are ejected when the RF amplitude reaches a point where the ion is at q_z=0.908 and thus the trajectory of the secular motion of the ion no longer falls within the stability diagram and the ion is no longer in the trap.[2] Ions with a lower m/z are ejected from the trap first. Ejection of the ions resulting from ramping the drive RF is referred to as mass selective instability scans.

The q_z parameter can also control the range of m/z(50-650) ions that can be stored and detected within the trap based on the amplitude of the drive RF. Low m/z ions are affected by a low mass cut-off(LMC) within the QIT. The LMC is a factor of the q_z level at which the drive RF amplitude is set. The LMC relates the q_z level of the RF and the mass of a specific ion of interest to the 0.908 ejection q_z level shown in Equation 8.[3]

$$\text{LMC} = \frac{\text{m} * q_z}{0.908} \tag{8}$$

The LMC is influenced by the q_z level at which the ionization and subsequent fragmentation occurs. The lowest m/z ion that is stored in the trap after ionization occurs must be stable at that q_z level that corresponds to the drive RF amplitude.

In the QIT, there also exists an upper mass limit of ions that can be detected in the ion trap due to the maximum voltage that can be applied to the ring electrode. The upper mass limit can be determined by the following relationship:

$$\frac{\text{m} * q_z}{\text{V}} = \text{constant} \tag{9}$$

The constant can be calculated from Equation 9 so that a value of 0.0797 is obtained. Since the maximum RF amplitude is approximately $15{,}000\text{V}_{(\text{p-p})}$ and the q_z necessary for ejection is 0.908, the maximum mass that can be detected is m/z 650. Higher m/z ions are thus stored in the trap, but cannot be ejected and detected due to the lack of RF amplitude that can be applied to the ring electrode in the QIT.[4]

Prior to detection, axial modulation is used to limit space charge effects that can occur during the mass-selective instability scan. Space charge effects occur as ions have electrical charges surrounding them and interact with each other by repulsion. In the QIT, this can cause lower m/z ions to reach the detector at different times, resulting in low resolution peaks, as the lower m/z ions are repelled by higher m/z ions that remain in the trap during the mass scan.[2] Axial modulation uses a $6\text{V}_{(\text{p-p})}$ supplementary oscillating frequency at half the frequency of the RF applied to the end cap electrodes. Axial modulation keeps the ions in a tight package when ejection occurs. While the QIT is considered a low resolution mass analyzer because the resolution is only unity, axial modulation helps to maintain unit resolution during detection.

Detection of ions within the QIT occurs, as mentioned earlier, as ions are ejected from the trap by increasing the drive RF amplitude shown in Figure 1.9. The detector used in a QIT is an electron multiplier which allows for a gain of 10^5 in intensity. The electron multiplier is generally a continuous dynode design shaped like a trumpet. Ions that are ejected from the trap are accelerated by an applied potential and strike the electron multiplier. A cascade of electrons then follows the 1.8 to $2kV_{(p-p)}$ potential that is applied along the multiplier. For each ion that strikes the multiplier, a gain of 10^5 is achieved shown in Figure 1.10. The detector is placed axially below one of the end caps and ions are then ejected axially in z axis during the mass selective instability scan and strike the detector.[1]

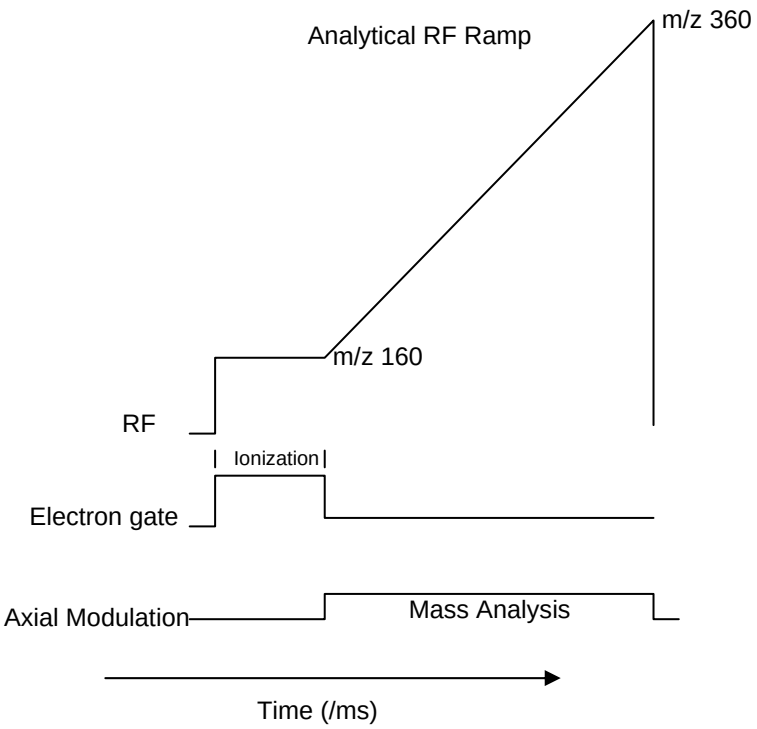

Figure 1.9. Mass selective instability scan.

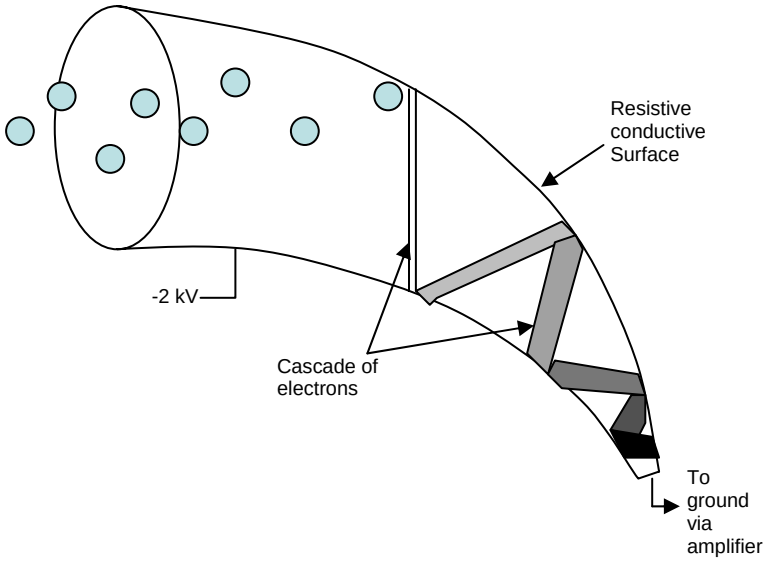

Figure 1.10. Electron multiplier.

The ability of the QIT to store and detect ions allows for many different applications in mass spectrometry. Tandem mass spectrometry(MS/MS) is a technique used frequently on a QIT. MS/MS is a complex process of performing essentially two mass selective instability scans on the same analyte within the trap. The theory of MS/MS analysis in a QIT will be discussed further in the next section.

Theory of Tandem Mass Spectrometry

MS/MS is a technique that essentially implies that MS analysis occurs twice within a QIT. The unique feature of MS/MS analysis is the ability to ionize molecules within the trap, isolate an m/z ion of interest, and then focus on the fragmentation of that one m/z ion. MS/MS occurs after ionization of the molecules when the precursor ion of interest is the only m/z ion stored in the trap with all ions of different m/z values being ejected. Since only the precursor ion is isolated within the trap, ions that are detected must be product ions that have fragmented from the precursor ion. Thus, noise from other background ions is minimized or eliminated.

In MS/MS analysis the first step is the isolation of a precursor ion by either broadband isolation or RF/DC isolation. Broadband isolation is the method of isolation used in most commercial instruments.[2-5] Broadband isolation uses a range of frequencies applied to the end cap electrodes, except for the frequency of the m/z ion of interest, causing ejection of all other ions. RF/DC isolation of the precursor uses the RF voltage to park the ion at a q_z of 0.78 when $a_z = 0$ so that the ion is at the base of the peak in the Mathieu stability diagram. A negative DC voltage is then applied to the ring electrode to increase the ion to an $a_z > 0$ in order to park the ion of interest in the apex of the stability diagram. The RF is then ramped in order to eject ions of lower m/z axially at $\beta_z = 1$, and the higher m/z are unstable radially at $\beta_r = 0$, thus isolating the ion of interest as depicted in Figure 1.11. The isolated ion can then be stored at any q_z level within the stability diagram for further analysis.[2-4]

After the precursor ion is isolated, the kinetic energy of the precursor ion is increased. In MS/MS, the energy of the selected precursor ion is increased by a process called collision induced dissociation or CID. CID occurs as the kinetic energy of the ion increases. The increase in kinetic energy causes the ion to oscillate with a greater amplitude within the QIT and collide with more helium atoms. The increase in kinetic energy of the ion creates more energetic collisions with the helium atoms. As the ion collides with the helium atoms, the internal energy of the ion increases until the internal energy becomes greater than the lowest bond energy and the ion begins to fragment.[2-6] Product ions that are detected after CID must have been produced by the precursor ion.

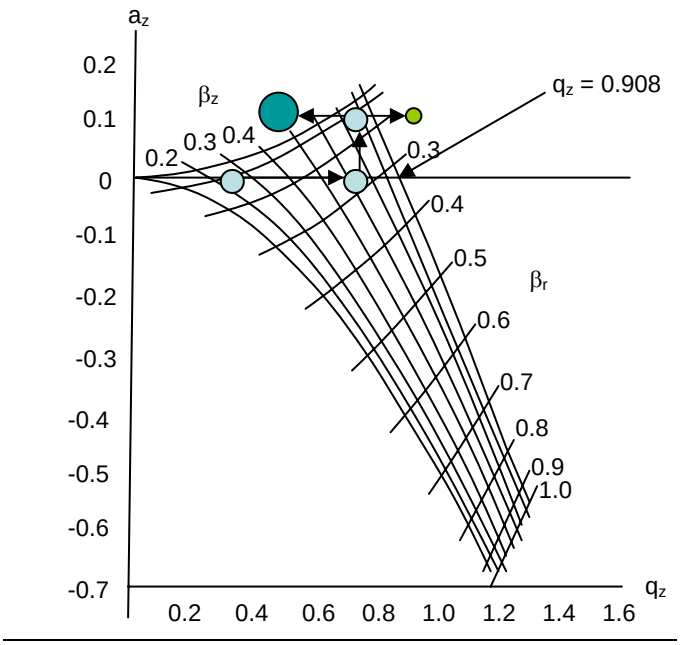

Figure 1.11. Principle of RF/DC isolation.

There are two types of excitation methods used for CID currently available on commercial instruments. The excitation methods are resonant and non-resonant excitation. In both cases, a potential is applied to the end cap electrode causing the amplitude of the motion of the precursor to increase. In non-resonant excitation, the ion cloud is excited by a low frequency dipolar pulse applied to the end caps. The application of the pulse forces the ions to move from the center of the trap toward one end cap. The ion then moves toward the other end cap with greater amplitude. The non-resonant excitation leads to CID by increasing the kinetic energy of the ion thus causing the ion to collide with more and more helium atoms.[5, 7]

Resonant excitation of the precursor occurs by applying a pulse with a frequency that is the same as the secular frequency of the ion of interest to the end cap electrodes. Resonance excitation causes the motion of the precursor ion within the trap to become resonant with the amplitude of the pulse. The ion motion increases as the amplitude of the pulse increases. The ion cloud collides with more helium atoms causing an increase in the internal energy of the precursor ion.

It is convenient to perform the CID process at a q_z of 0.4 where it is optimal to cause an increase in the kinetic energy of the precursor ion without ejecting it from the

trap. During the CID process, the drive RF amplitude is set to a q_z of 0.4 so that there is a balance between the amount of kinetic energy forced into the ion and the depth of the pseudo-potential well within which the ion is stable. Setting the RF amplitude to correspond to a q_z of 0.4, moves the ion cloud to the most stable point in the stability diagram. At a q_z of 0.4 it is also possible to hold on to many of the product ions that are formed from the CID process. However, some low m/z ions will not be stable because the RF amplitude will correspond to a $q_z > 0.908$ for these m/z ions. Therefore, the low m/z ions will no longer be in the trap. The low mass cut-off becomes a problem when attempting to analyze low m/z fragment ions in MS/MS analyses.

As much as Chapter One was focused primarily on the operation of the QIT as a mass analyzer, Chapters Two and Three will focus on research performed primarily by the author to elucidate other properties of the QIT. Chapter Two is devoted to a presentation on the research on the motion of the ions within an ion trap. Chapter Three will be focused on research that eliminates the low mass cut-off in QIT MS/MS analysis.

In Chapter Three of this work, there will be a discussion of research performed in our group on solutions to the LMC during MS/MS analysis in a QIT. Other research has been done to extend or eliminate the LMC by experimenting with the CID process and q_z level at which CID occurs.[8-10] One method that helps to extend the low mass cut-off is that of operating the CID process at a lower q_z, generally 0.25. For some LC-MS/MS systems, the q_z is set to 0.25 for the CID process. However, many ions still fall below the low mass cut off when the peptides are of larger m/z and increased fragmentation of the precursor ion can occur due to the increase in internal energy during the CID process.[11] The lowering of the q_z is used as a solution to the problem of the LMC. Other attempts to extend the LMC have been limited to manipulating the drive RF frequency.[12]

CHAPTER 2

Ion Mobility Based Separations within a Quadrupole Ion Trap

Introduction:

Separation of ions in a quadrupole ion trap based on the phase relationships of the secular frequencies of the ions has potential for eliminating the need for poor chromatographic separations of molecules such as isomers. Isomeric ions are ions that have the same structure and m/z ratio. Separation of isobaric ions, or those with the same m/z ratio, but totally different structures is useful for the same reason. Ion mobility based separations in a quadrupole ion trap can be quite useful for analyzing isobaric ions in a QIT based on the unique motion of the ions.

Traditional ion mobility experiments generally take place in drift tubes. However, ion mobility experiments in a QIT have a unique advantage over traditional ion mobility studies in that ions can be stored over a longer period of time and can be manipulated with imposed electrical pulses. The ion's reaction to these manipulations can then be studied. The research presented in this paper focused on modifying an existing commercial GC/MS instrument for ion mobility studies.

Ion mobility spectrometry(IMS) has been around since the early 1970's. In IMS experiments, ions are separated in a drift tube based on mass, charge, and collisional cross section. The separation can be achieved because the ions are given the same kinetic energy by using an applied potential. In the drift tube, ions collide with neutral drift-gas molecules, the number of which determines the average velocity, ν_d(cm s^{-1}). The average velocity is directly proportional to the applied electric field strength: $\nu_{drift} = KE$ where E is the electric field strength (V cm^{-1}) and K is the ion mobility constant (cm^2 V^{-1} s^{-1}). The ion mobility constant depends on both the nature of the ion and the drift-gas.[13-15]

IMS has been confused with mass spectrometry, especially for time-of-flight mass spectrometry(TOF-MS). Differences between the two include, IMS operates at atmospheric pressure and suffers from a much lower peak resolution than in TOF-MS. However, instruments have been developed for IMS studies by combining mass spectrometers such as the quadrupole ion trap and TOF-MS to existing IMS instruments. While the motion within a QIT is more complex than in either IMS or TOF-MS

instruments, research based on these IMS experiments has been conducted in order to elucidate the axial motion of ions within the trap.[16-18]

The mobility of an ion in a QIT is dependent on the temperature of the trap, the pressure of the helium inside the trap, the ion charge, reduced mass, and collisional cross section of the ion. In a high pressure(~1 mtorr) helium environment, ions collide with helium molecules at an increased frequency compared to low pressure environments. More collisions with helium atoms will lead to an increase in the internal energy of the ion as compared to a low pressure helium environment. An increase in temperature of the trapping environment will cause a greater increase in the kinetic energy of the helium atoms, thus each subsequent collision with helium atoms will lead to a greater deposition of energy into the ion. In commercial instruments, the temperature and pressure are held constant and as a result, have no influence on the ion mobility.[16, 18]

The study of the axial motion of ions in the QIT is termed ion tomography. Tomography experiments have been developed that involve the mapping of the ion motion within the mass analyzer and have been the focus of previous research on ion mobility within the quadrupole ion trap. The trajectory of iron and aluminum was studied by Wueker who photographed the ions.[19] The first group to do laser induced fluorescence studies on atomic ions to determine the size of the ion cloud was Knight and Prior.[20] Tomography experiments have been developed to study the motion of ions within the quadrupole ion trap. Laser based tomography experiments were the first tomography experiments in a QIT to gain popularity and have been able to even obtain spatial information on the position of the ion cloud by measuring the photo-dissociation products as a function of laser beam position.[17, 21, 22]

Development of new techniques for tomography experiment has been developed because of the negative effects of laser based methods. The most negative effect being the distortion of the electrical field in the trap from the modification of the physical components of the trap. For laser based tomography experiments, it is necessary to drill holes in the end-cap for the laser which can distort the electric field. Therefore, both AC and DC pulse tomography experiments have an advantage over laser probing experiments because it is unnecessary to modify the trap.[16, 17]

Tomography experiments incorporate isolation of a precursor ion, excitation of the ion, and ejection and subsequent detection of the ion. Isolation of the precursor ion can be achieved by either broadband isolation or RF/DC isolation. Excitation of the mass selected ion is achieved generally by either resonant excitation[3, 5, 23, 24] or non-resonant excitation much like in the CID process mentioned in Chapter 1.[16-18] Resonance excitation in tomography experiments employs an AC pulse applied to the one end cap electrode. The AC pulse has a radio frequency resonant with the secular frequency of the selected ion and is used to position the ion cloud away from the center of the trap. After the displacement of the ion cloud, a $100V_{(0\text{-}p)}$ DC pulse is applied to the other end cap electrode and used to re-position the ions in the opposite direction of the initial AC pulse prior to detection.[16, 17, 21]

Another method for displacing the ion cloud off center is a non-resonant excitation technique termed DC tomography. DC tomography experiments use two DC pulses to track the trajectory of an ion over a period of time. A $9V_{(0\text{-}p)}$ "tickle" pulse is used to excite the ions coherently and move the entire ion cloud from the center of the trap by an increase in kinetic energy. The coherence of the ions within the ion cloud is important in tomography studies when attempting to study the secular motion of specific m/z ions. Therefore, the use of the "tickle" pulse must not cause any incoherence of the ion cloud upon excitation.

The DC pulse is considered a broadband excitation method because it is a non-resonant excitation technique that excites all ions stored in the trap when the pulse is applied to the end-cap. Another high voltage($\sim 100V_{(0\text{-}p)}$) DC pulse is then applied to the opposite end-cap and used to re-position the ions before detection. The location of the ion cloud in the trap at any given time after the "tickle" pulse is applied can be determined by the intensity of the peak of the ion in the mass spectrum. A greater intensity would suggest that the ion cloud remained in the trap after the $100V_{(0\text{-}p)}$ pulse was applied. Should the intensity be near zero, this suggests that the entire cloud was ejected prior to detection.[16-18]

The cooling time is the time it takes for the ion cloud to return to the center of the trap after excitation. Ions with different m/z and collisional cross sections stored in an ion trap have different cooling times. Larger m/z ions will have shorter cooling times as

they will move shorter distances from the center of the trap upon excitation as compared to smaller m/z ions. This is due to the fact that heavier ions do not react as quickly as lighter ions to the potential applied to the end cap.[24-26]

The study of the motion of the m/z 106 molecular ion from the *o,m,p*-xylene isomers and the m/z 105 product ion was carried out using DC tomography and the results presented here. Based on the tomography experiments, it should be possible to measure the cooling time of the ions. The goal of this experiment was to separate the m/z 105 and 106 ions based on cooling times and the secular frequency of the respective ions.

The separation of isomeric ions by DC tomography should be possible if the ions of interest have a different phase relationship in their secular frequencies. Since the collisional cross-section of each of the isomeric ions is different, there should be a difference in the phase relationship. Ions that have the same m/z value, but differ in structure are termed isobaric ions and the separation of these ions based on the phase relationship of the secular frequencies of the ions can be seen.

Experimental:

Chemicals used in this experiment consisted of *o,m,p*-xlyene purchased from Sigma-Aldrich. Instrumentation used for the DC tomography experiments consisted of a modified Varian Saturn 4D GC/MS shown in Figure 2.1. Modifications made to the GC/MS were required to obtained control over timing of the pulsing events and for control over the amplitude of the DC pulses. One of the two leads to the end cap electrodes was connected to a transistor-transistor logic(TTL) switch box. The other lead was connected to a pulsed high voltage power supply.

Control of timing over the experiment was possible using a custom built timing circuit consisting of a phase lock circuit shown in Figure 2.2 which phase locks the RF from MS electronics, the TTL pulse used to start the acquisition process, and a digital delay generator(DDG)(Stanford Research Systems, Inc. Model No. DG535) shown in Figure 2.3. The TTL pulse that used to start the acquisition process was sent to the DDG which then controlled the time at which the end cap connected to the high voltage DC power supply was to fire. The DDG also controlled the above mentioned TTL controlled

switch box, shown in Figure 2.4, and was used to switch the potential applied to the end-cap from the constant application of the RF to the $9V_{(0\text{-}p)}$ DC "tickle" pulse.

Ion Trap Data Station V1.31 software was programmed to generate the TTL pulse that was sent to the phase lock circuit. The phase locked signal was then sent to the DDG where the delay times between the $9V_{(0\text{-}p)}$ DC "tickle" pulse and $100V_{(0\text{-}p)}$ DC probe pulse were synchronized. The $9V_{(0\text{-}p)}$ DC "tickle" pulse was switched between RF and DC by the TTL pulse sent from the DDG to the TTL switch box as mentioned above.

The xylenes were introduced into the trap via a FinniganMAT designed vacuum driven gas delivery system shown in Figure 2.6. The system consisted of two needle valves and a vacuum that was used to eliminate excess xylene vapor from entering the trap. The needle valves gave even greater control over the amount of vapor that entered the trap. The vapors from the analyte head space were pumped into the manifold of the QITMS. It was again not possible to measure the pressure of the analyte in the trap or manifold. Helium entered the trap via the GC, therefore the helium pressure was not monitored other than by the pressure gauge inside the GC.

Finally, an RF/DC isolation technique was used to isolate the m/z 106 molecular ion and the m/z 105 product ions from the xylenes in separate experiments. The conditions used to isolate the ions were the same. The m/z 105 and 106 ions, shown in Figure 2.7, were isolated at a q_z=0.8 and an a_z equivalent to the $-50V_{(0\text{-}p)}$ DC pulse applied to the ring electrode. In order to insure the ions were sufficiently cooled to the center of the trap after the RF/DC isolation, the ions were allowed to cool for 25ms before the mass scan.

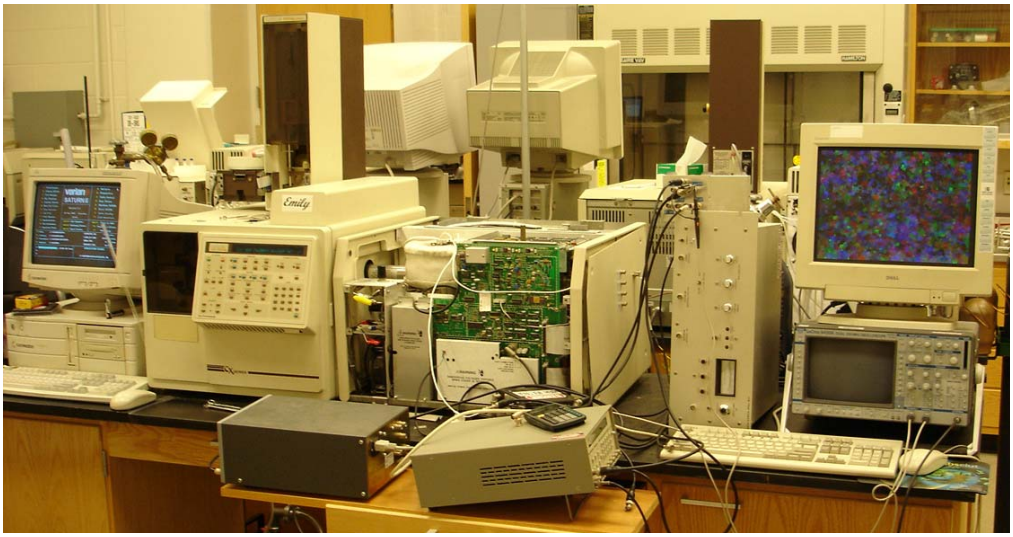

Figure 2.1. Modified GC/MS.

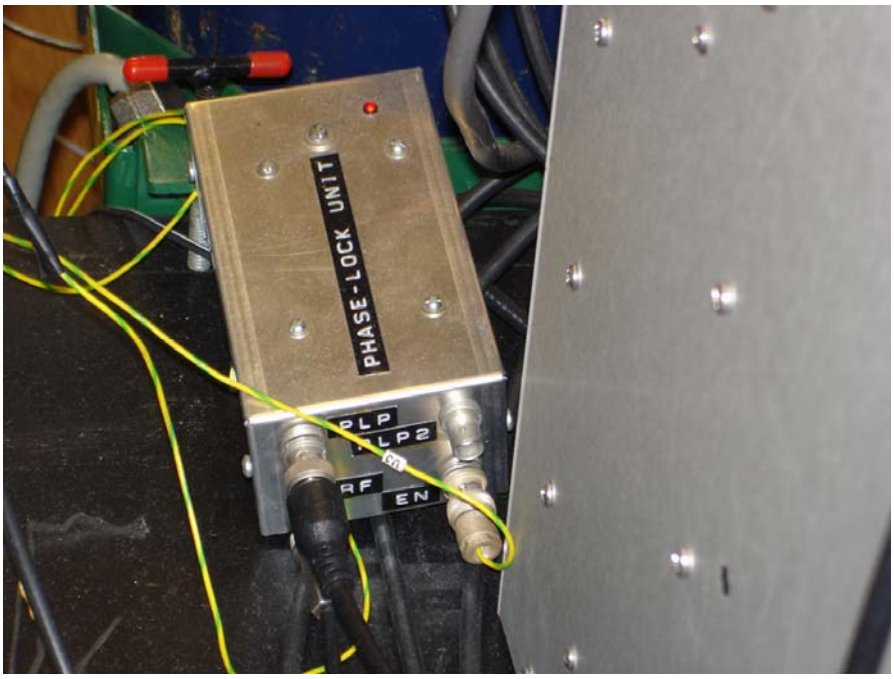

Figure 2.2. Phase lock unit.

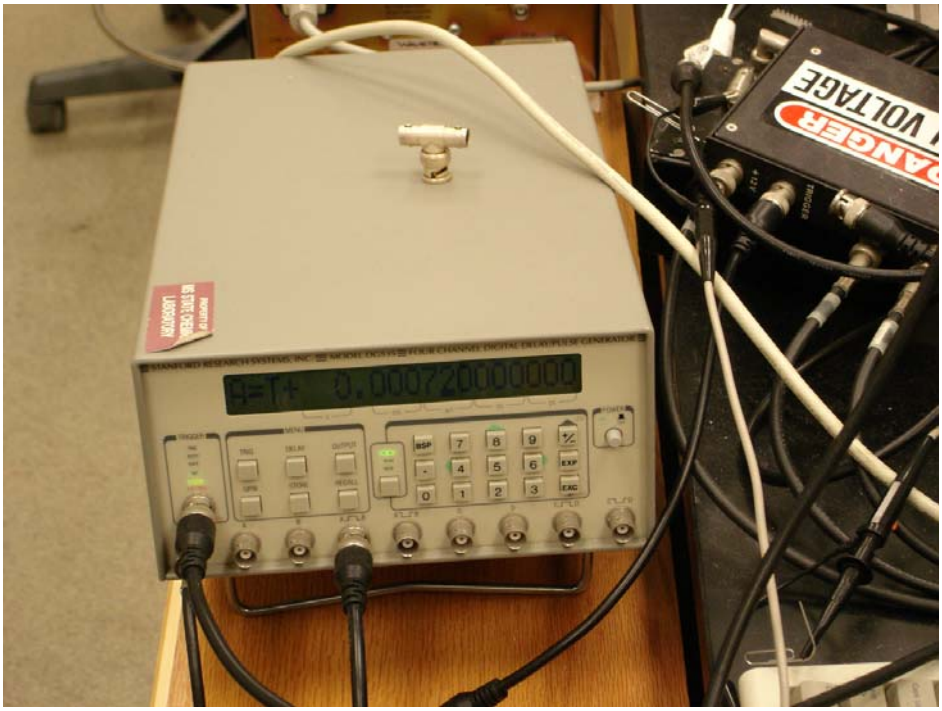

Figure 2.3. Digital delay generator.

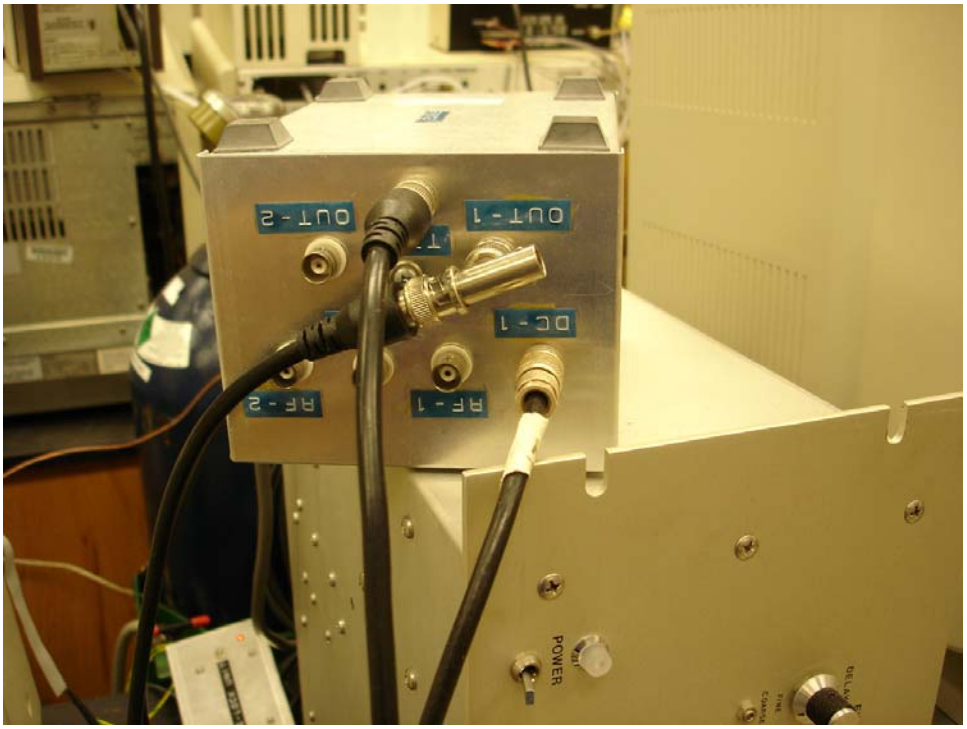

Figure 2.4. TTL switch box.

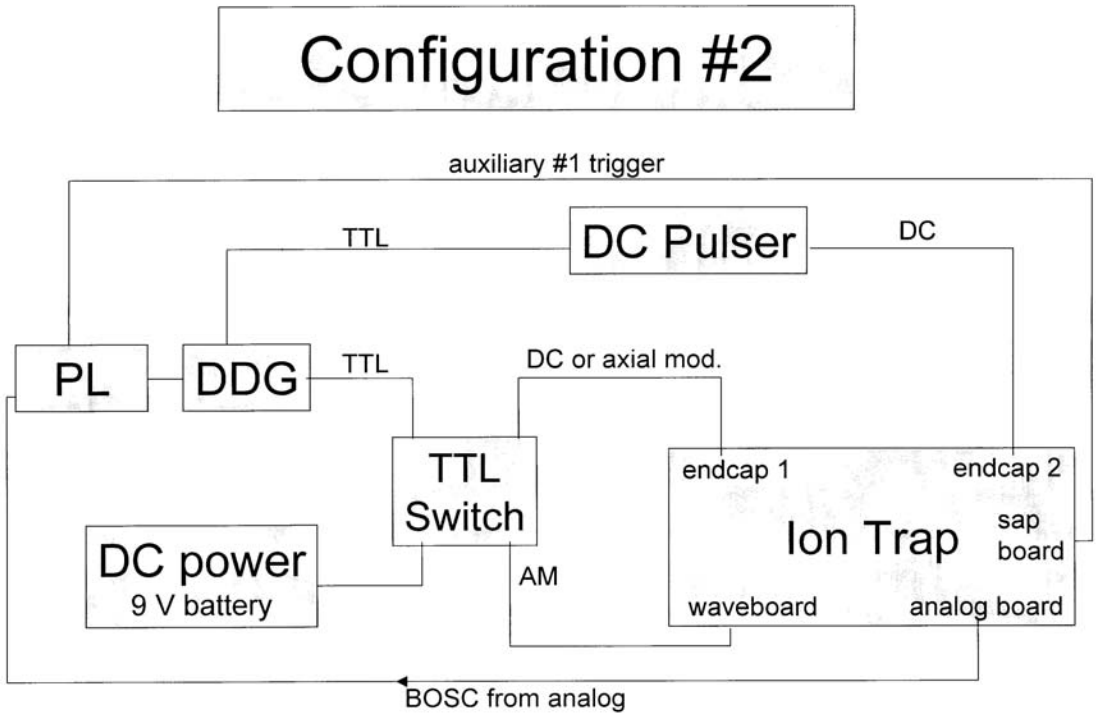

Figure 2.5. Circuit diagram for DC tomography experiment.

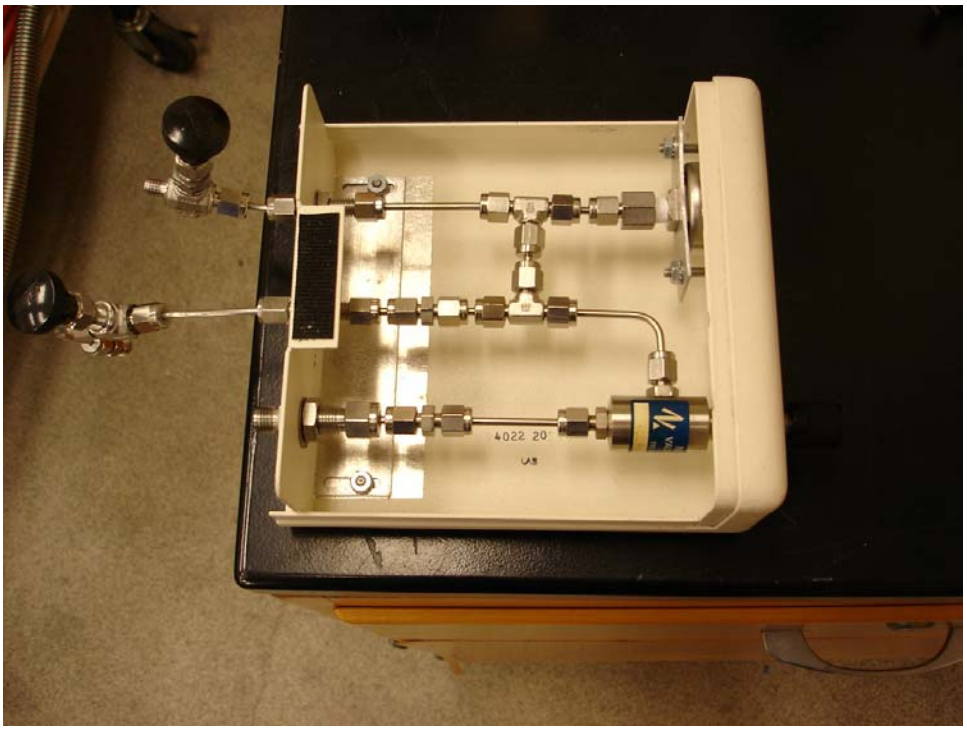

Figure 2.6. FinniganMAT vacuum delivery system.

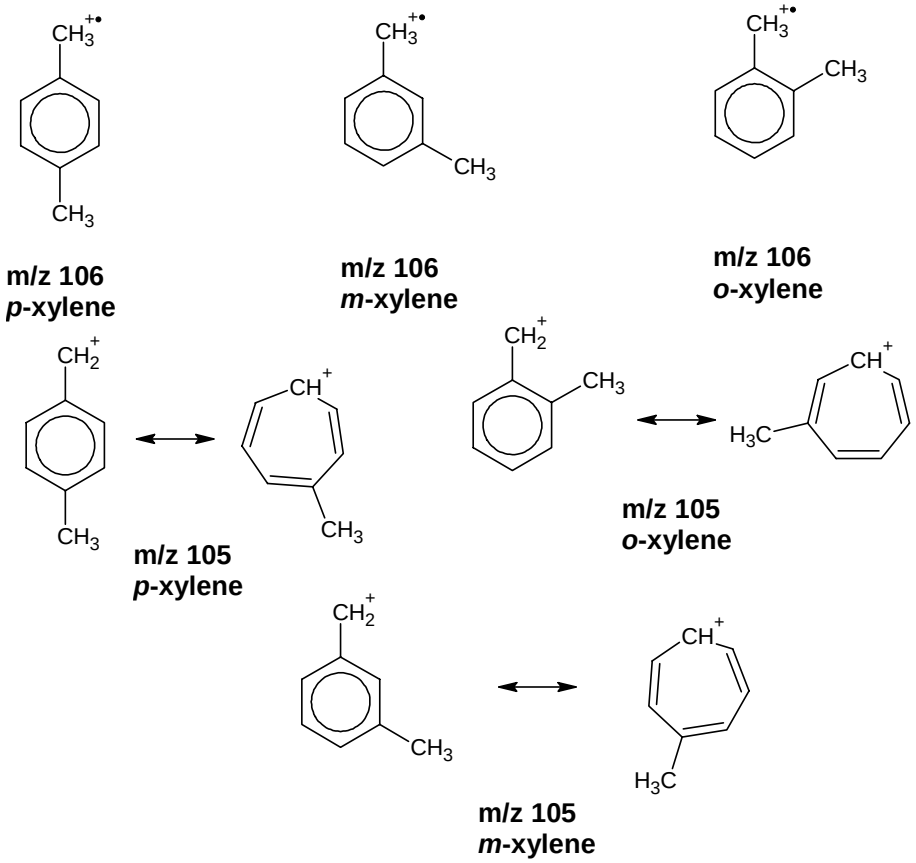

Figure 2.7. Xylene isomers and corresponding ions m/z 106 and 105

Results and Discussion:

A $9V_{(0\text{-}p)}$ "tickle" pulse was used to coherently excite the ion cloud increasing the amplitude of its orbit of motion within the trap shown in Figure 2.8. The $100V_{(0\text{-}p)}$ DC pulse was used to eject half of the ion cloud once the ions had cooled for 23ms after the initial $9V_{(0\text{-}p)}$ "tickle" pulse was applied. If the ion cloud was moving toward the end cap that had the $100V_{(0\text{-}p)}$ DC pulse applied then the pulse would stop the ion cloud in the trap. Should the ion cloud be located near the opposite end cap then the cloud would be ejected prior to detection and the intensity in the mass spectrum should be near zero.

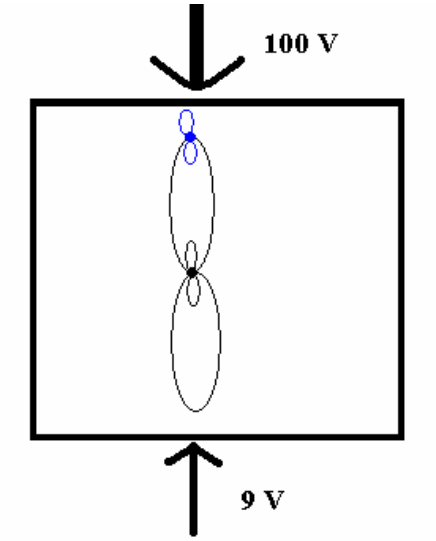

Figure 2.8. DC pulses used for DC tomography.

Using DC tomography allowed the measurement of the secular frequencies of both the m/z 106 and 105 ions from each of the xylene isomers based on the intensity of the ions at a given delay time between pulses. The graph of the secular frequency of the m/z 106 ion from *p*-xylene showed the sinusoidal motion of the m/z 106 ion within the ion trap shown in Figure 2.9. The peaks along the edge of the plot were actually the drive RF frequency superimposed on the motion of the ion. The measurement of the motion was taken with a delay time interval between the "tickle" and probe pulses of 150 -185μs. Both the *m* and *o*-xylene m/z 106 ions exhibited the exact same frequencies as the m/z 106 from *p*-xylene and were therefore not presented here. At longer delay times between the "tickle" and probe pulses, the oscillation of the secular frequency collapses to near zero and only exhibits the drive RF superimposition otherwise termed micro-motion. The same micro-motion cause by the drive RF superimposition can be seen in the graph of the secular frequency of the m/z 105 ion from *p*-xylene shown in Figure 2.10.

A cooling curve which shows the amplitude of the ion cloud motion back to the center of the trap was then obtained by acquiring data after adjusting the delay time between the "tickle" pulse and the 100 $V_{(0\text{-}p)}$ probe pulse from 50 μs to 1 ms. Data points were acquired after every five full mass scans, the delay between pulses was increased by 500 ns until three full oscillations of the ion cloud have been mapped. The data points formed a wave that had a wavelength of ~30 μs shown again in Figure 2.9 for the m/z 106 of *p*-xylene.

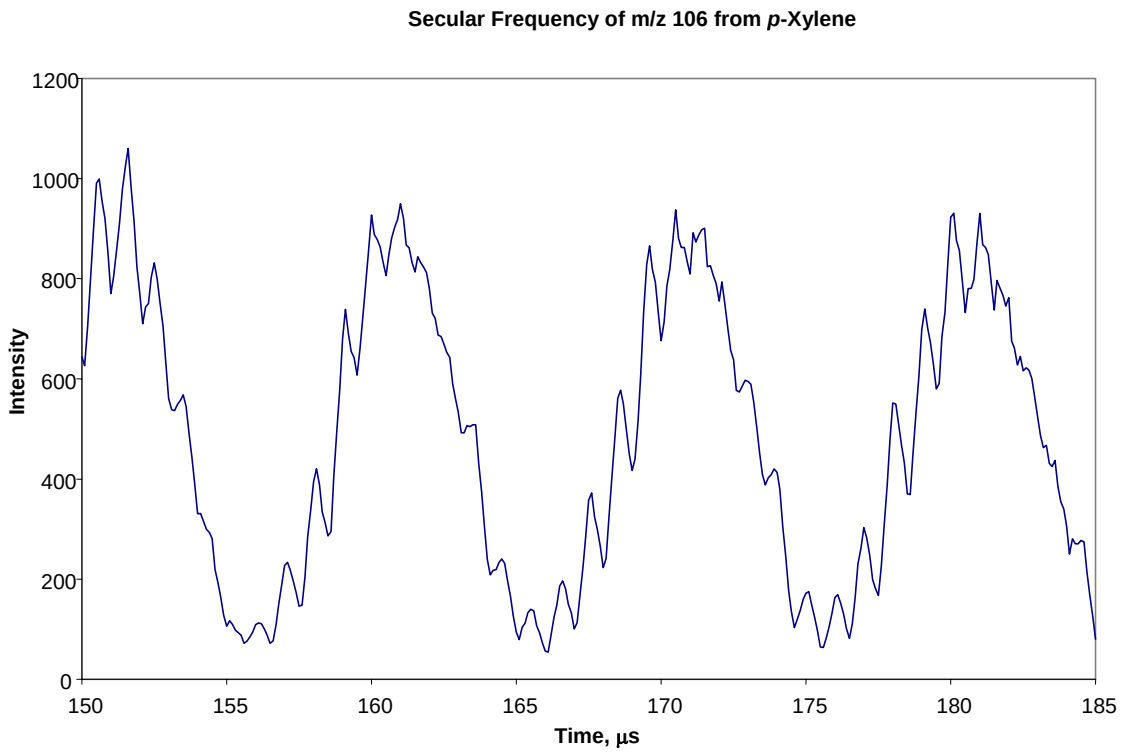

Figure 2.9. Secular frequency of m/z 106 from *p*-xylene.

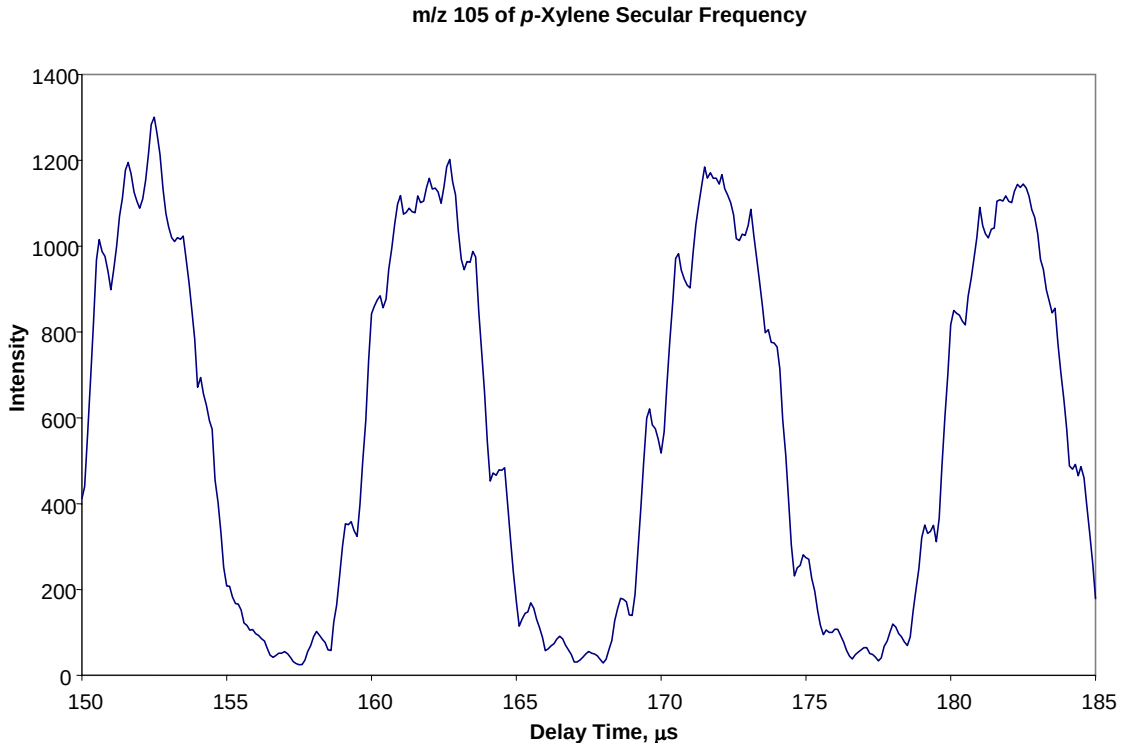

Figure 2.10. m/z 105 from *p*-xylene secular frequency.

The delay time was then incremented by 100 μs between experiments. The raw data shown in Figures 2.11 and 2.12 for the cooling curve was obtained from the tomography study of the m/z 106 and 105 ions motion from *p*-xylene collected at time intervals of 50, 150, 250, 350, 450, 550, 650, 750, 850, and 950 μs. From Figure 2.10, it was apparent that the amplitude of the oscillation of the m/z 106 ion was greatest immediately after the "tickle" pulse was fired corresponding to a delay time of 50 μs. The graph also showed the effect of the cooling of the ion cloud to the center of the trap as the amplitude of the oscillation of the secular motion decreased at longer times.

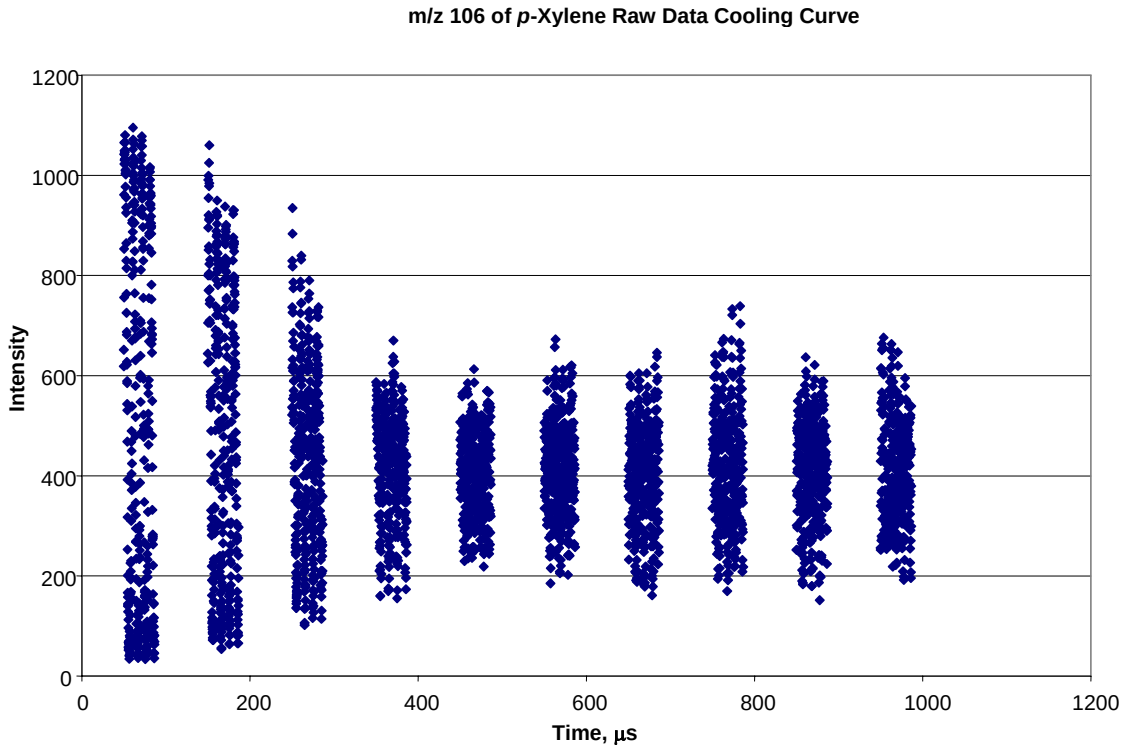

Figure 2.11. m/z 106 of *p*-xylene raw data cooling curve.

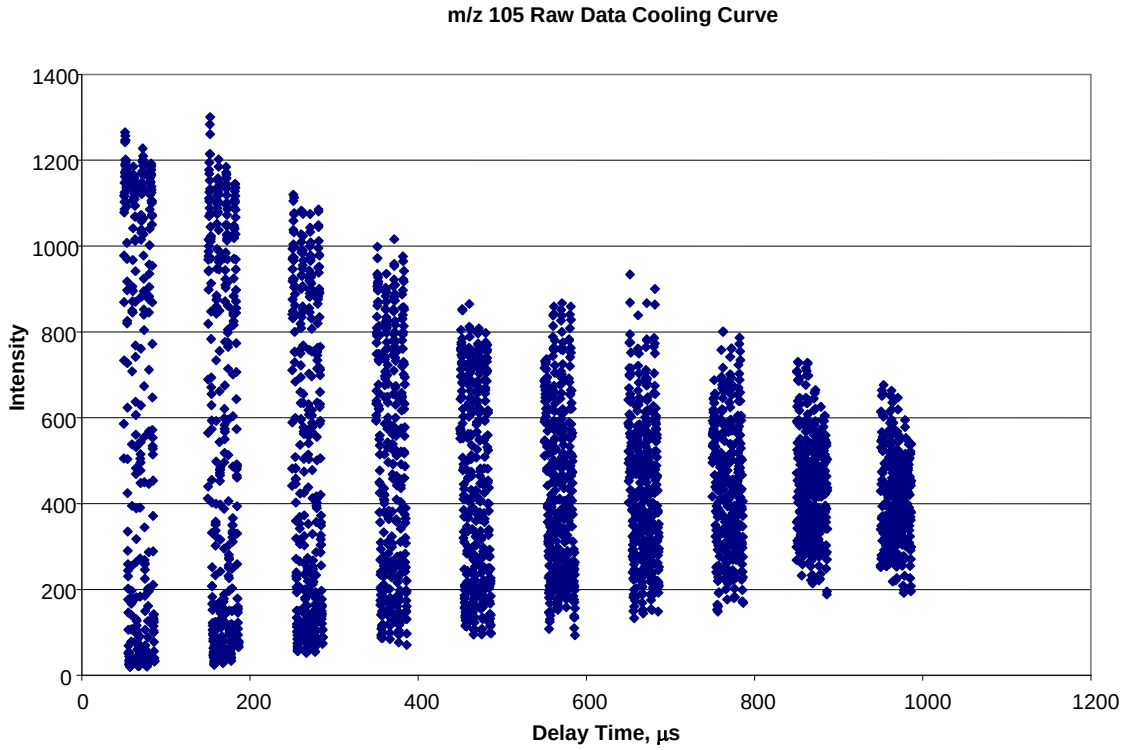

Figure 2.12. Raw data cooling curve for m/z 105.

Figure 2.13 displays a smoothed cooling curve plotted for the m/z 106 ion from *p*-xylene. The maximum intensity was determined by the average of the three peaks from the measured oscillation shown previously in Figure 2.9. The averaged maximum intensity was plotted versus time. The cooling time for each of the m/z 106 ions from each xylene was less than 400 µs. No differences were seen in the cooling curves of each m/z 106 ion from the different xylenes shown in Figure 2.14 and therefore suggested that the collisional cross section for each isomeric ion was too similar to be differentiated in a QIT. The cooling times appeared to be the same, and therefore the mobility of the ions must therefore be the same.

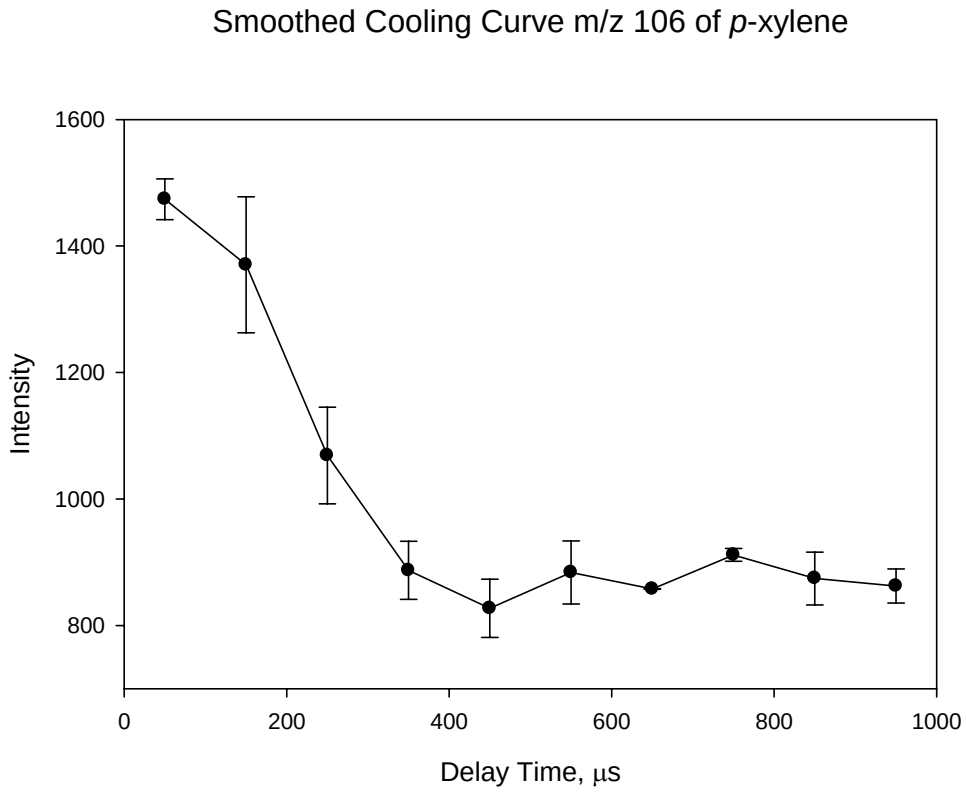

Figure 2.13. m/z 106 from *p*-xylene smoothed cooling curve.

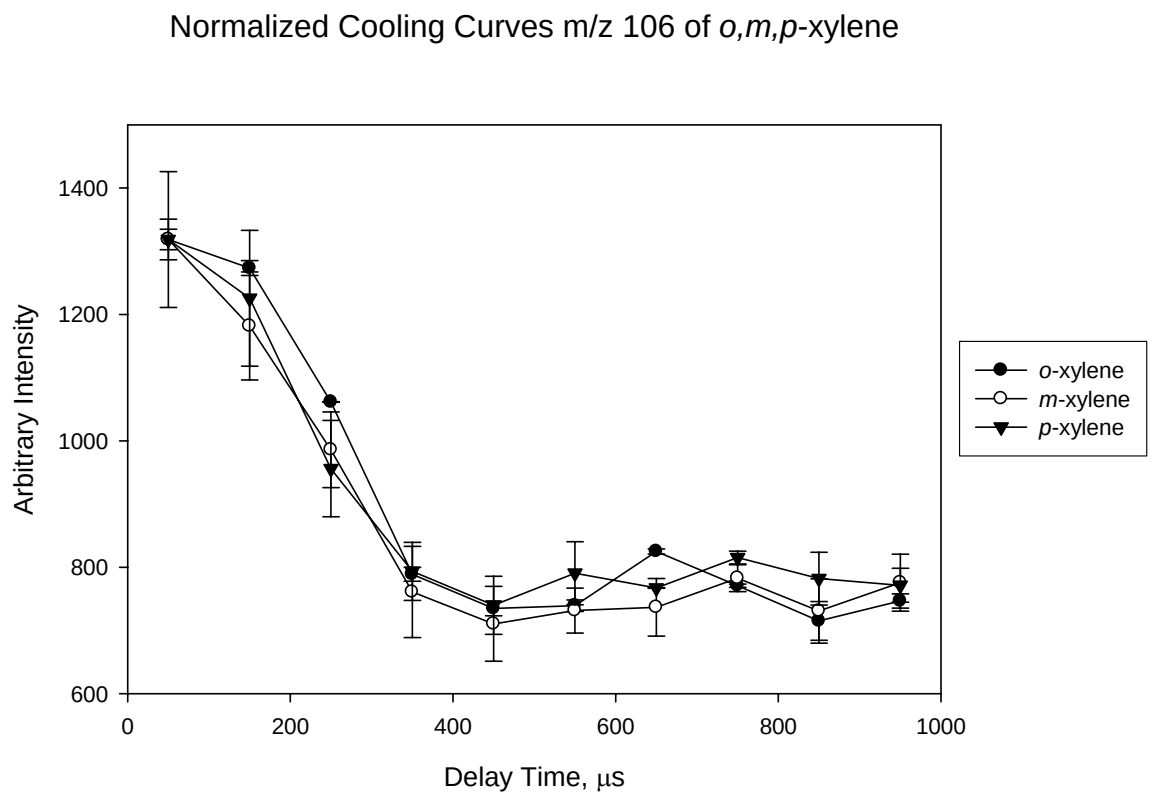

Figure 2.14. *o,m, p*-xylene m/z 106 cooling curves.

Cooling times less than 600 μs were expected for the m/z 106 ions as previous studies showed that for the m/z <106, the cooling time was greater than 600 μs. The above results showed the effect of ion size on the ion mobility within the QIT. The larger m/z 106 ion from *p*-xylene was predicted to be less displaced by the $9V_{(0\text{-}p)}$ tickle pulse compared to the m/z 105 from *p*-xylene and thus have a shorter cooling time. Empirical results confirmed that hypothesis as shown in Figure 3.14. The m/z 105 ion from the *p*-xylene has a cooling time of approximately 450 μs which was at least 50 μs longer that the m/z 106 ion from the *p*-xylene.

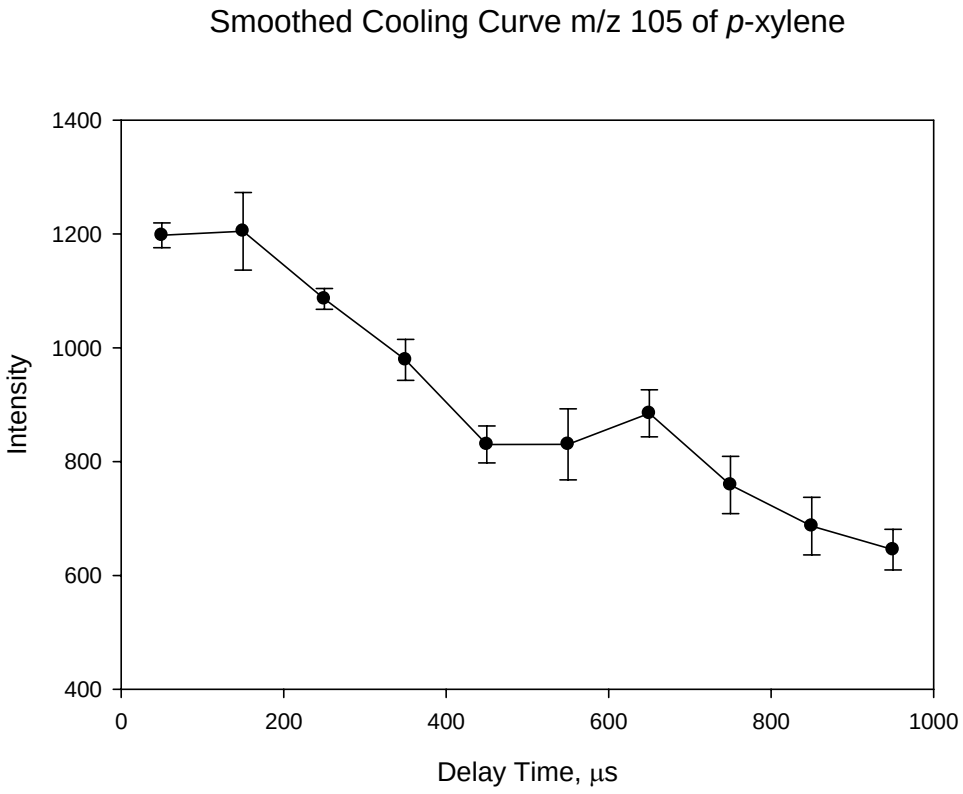

Figure 2.15. Smoothed cooling curve for m/z 105 ion from *p*-xylene.

The axial location of the ions within the trap also elucidated the property of how much kinetic energy an ion has at a given time. DC tomography allowed for the tracking of the trajectory of the ion motion of the xylene isomers without modification to the ion trap. The study of the ion trajectory could be used to potentially separate molecular ions from isomeric compounds based on the collisional cross section of each ion. DC

tomography experiments are useful in gaining information on what effect the pressure of the helium has on the motion of the ion. The effect of the trap temperature on the motion of the ion can also be studied by the ion tomography experiments. Ion tomography experiments are most useful in determining the effects of the collisional cross sections of different ions on the mobility of the ion when all other factors are kept constant.

From the plot of ion intensity versus the time interval between the initial "tickle" pulse and the probe pulse shown in Figure 2.15, it was apparent that the m/z 105 ion from *p*-xylene was excited in the same way as the m/z 106. The fact that the m/z 105 ion was not moved from the center of the trap could be due to several factors. These factors include that the "tickle" pulse was of too low an amplitude to force the ions to move, or it could be due to the fact that the m/z 105 are larger than ions previously studied in other reports.[17] The latter being plausible because it is well known that larger ions do not have as great a mobility within the QIT as smaller m/z ions. It could also be due to the pressure of the helium or the pressure of the neutral xylenes within the trap limited the mobility of the ions.

After obtaining the cooling curves and secular frequencies of the ions, the goal was separation of the isomeric m/z 106 ions from each xylene based on some slight difference in secular motion within the QIT. The separation turned out to be unsuccessful because the secular motion appeared the same for each of the m/z 106 ions shown in Figure 2.16. Separation of ions with DC tomography is possible if one of the time increments shows any points along the curve that indicates the motion of the ions was out of phase. DC tomography was able to separate ions of different m/z ratios as shown in Figure 2.17 for the m/z 105 and 106 ions from *p*-xylene. While these different m/z ions were somewhat out of phase, it appeared from the above results that the cooling times and secular frequencies for the isomeric m/z 106 ions were the same and thus further separation was not possible.

In the case of ions of different m/z ratios, from Figure 2.17 it can be seen that DC tomography can be used as another quasi-separation technique much like other existing chromatographic techniques. The separation of ions of different m/z ratios was possible because of the differences in the secular frequencies whereby the frequencies are out of phase relative to each other. At certain delay time intervals between the two DC pulses,

it should be possible to completely eject one ion while the other is still stored. The delay time of 155-160 μs shown in Figure 2.17 would be a perfect example of a delay time interval in which frequencies of the m/z 105 and 106 from *p*-xylene are slightly out of phase. At this delay time interval it should be possible to separate the respective ions.

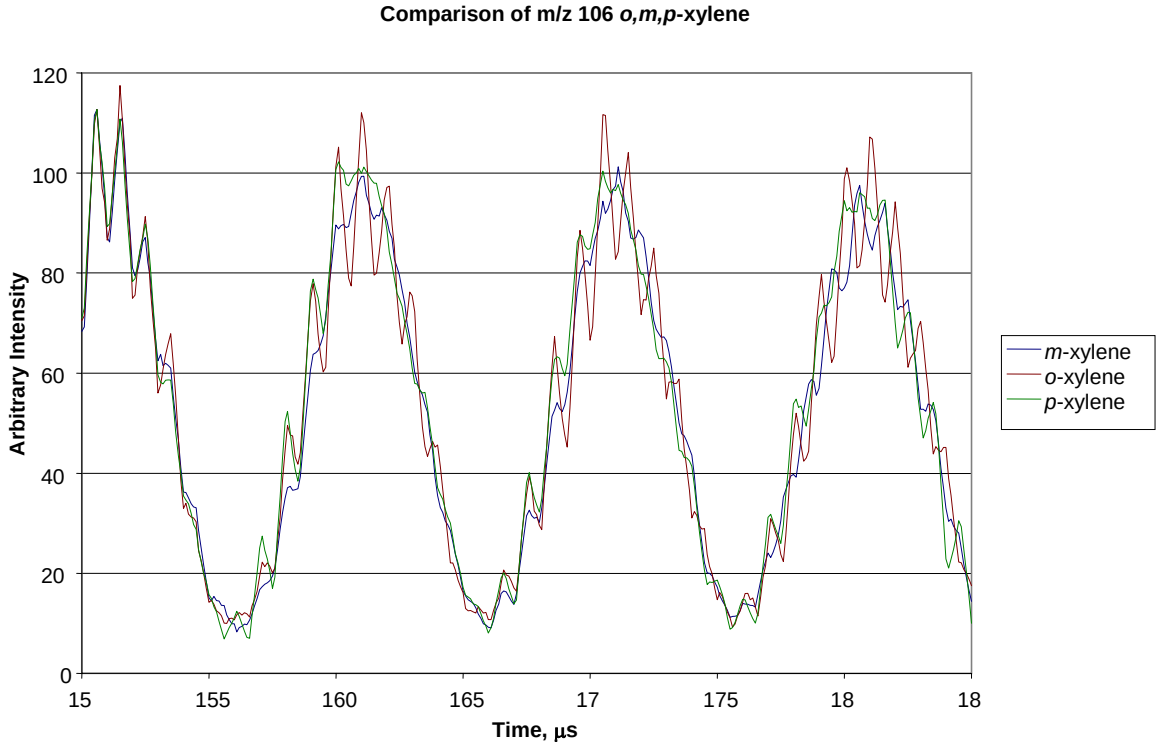

Figure 2.16. Comparison of m/z 106 ions from each xylene isomer.

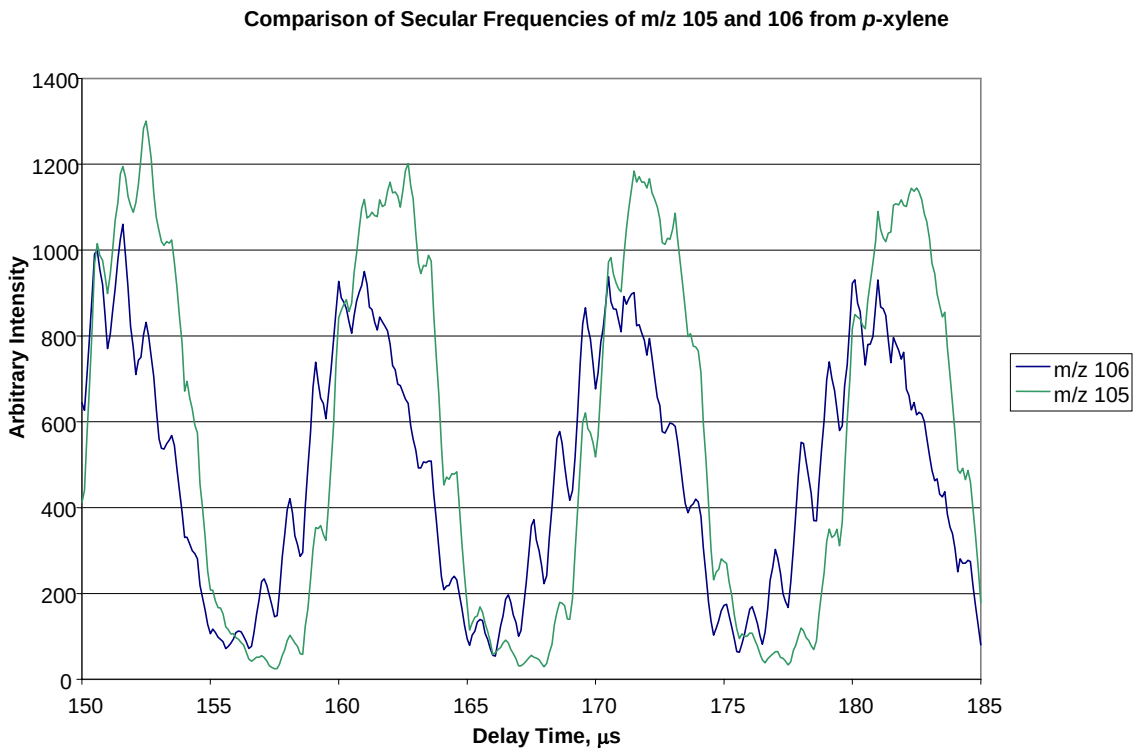

Figure 2.17. Comparison of the secular frequencies of m/z 105 and 106 from *p*-xylene.

The conclusion to the tomography experiment was that DC tomography on our modified GC/MS was unable to separate the isomeric m/z 106 ions from the xylene isomers. However, DC tomography did allow for the separation of ions with different m/z ratios as shown in Figure 2.17. Obtaining information on the ability of DC tomography to separate isobaric ions which have the same m/z but different chemical structure would confirm the usefulness of this separation technique. DC tomography is still a useful and novel method of studying the axial motion of ions as the results were printed here.

CHAPTER 3

High Amplitude, Fast Collisional Induced Dissociation in a Quadrupole Ion Trap Mass Spectrometer

Introduction:

The need for the analysis of low m/z ions is great in the field of proteomics. For peptide sequencing, the detection of low mass immonium ions can facilitate identification of specific amino acids in a peptide. Unfortunately, quadrupole ion traps have a difficulty analyzing low mass ions due to the low mass cut-off. The technique of Pulsed Q Dissociation(PQD) described by Schwartz and coworkers involves isolation of the precursor ion at a q_z of 0.4 and use of a short(50-300 μs) pulse for CID and dropping the q_z to 0.1 100 μs after the CID pulse in a linear ion trap. Low m/z ions remain stable in the trap at the lower q_z value immediately before detection.[9] PQD allows for the detection of the ions that would normally fall below the low mass cut-off from the CID process when $q_z = 0.4$.

In a quadrupole ion trap, the ability to analyze low m/z ions can elucidate the composition of organic molecules which could be used as markers for the identification of compounds in complex mixtures. Therefore, further exploration of the processes and energetics of high amplitude, fast collision induced dissociation combined with pulsed q were explored in this work. Elucidation of the inner workings of the CID and pulsed q processes would allow optimization of the technique and provide a routine analytical tool. The ability to analyze the low mass fragments of small organic molecules in MS/MS analyses would allow for a greater understanding of the structural composition of the analyte. No reviews on PQD have been published as of the publishing of this thesis. Therefore the research presented here contains a very detailed description of the high amplitude, fast CID process combined with pulsed q method which is similar to but presented in more detail than PQD.

Experimental:

Chemicals used in the experiment consisted of FC-43 calibration gas available on our GC/MS, n-butylbenzene purchased from Sigma Aldrich, chlorpyrifos purchased from Chem Services, and isoleucine purchased from Sigma Alrich. Sample introduction into the system for the FC-43 calibration gas was carried out by bleeding the head space directly into the QIT. Chlorpyrifos and n-butylbenzene were introduced by GC. Isoleucine was derivatized with a 1:1 BSTFA/Pyridine solution for 15 minutes at 40^{o}C. The derivatized amino acid had a molecular weight of 275 Da and was introduced by GC.

A modified Varian Saturn 4D GC/MS was used for the pulsed q experiment. The major modification employed the use of monopolar CID in which only one of the end caps has the CID pulse applied. A digital delay generator(DDG)(Stanford Research Systems, Inc. Model No. DG535) was used to control the timing on the modified instrument. A Universal Waveform Generator(Wavetek Model No. 39) was used to generate the resonance excitation pulse used for CID in the monopolar mode. There were no physical modifications to the instrument when run in the dipolar CID mode.

The Ion Trap Data Station V.1.31(ITD) software was used to create a program that would allow for manipulation of the control of the MS analysis on the QIT. The software allowed manipulation of the voltage and pulse width during the CID process. The software also allows the setting of the delay time between CID and the lowering of the q. The ITD software also controls the lowering of the q_z level immediately before the mass selective instability scan.

Results and Discussion:

Parameters for using the high amplitude, fast CID were explored to achieve results comparable to conventional CID. The CID voltage, RF amplitude, and their corresponding frequencies were measured with an oscilloscope. There was a 160 μs delay between when the software calls for an increase or decrease in RF amplitude and the actual RF response shown in Figure 3.1. Since the lag time in RF operation was present in the commercial set up, it was necessary to use the DDG to gain better control over the timing of pulses within the experiment. Better control over the timing was achieved by generating a CID waveform using the waveform generator and using a TTL

pulse to trigger when the CID waveform is applied to the end cap. The CID waveform had to be resonant with the secular motion of the ion of interest within the trap as mentioned in Chapter 1,[5] therefore at a q_z of 0.4 the frequency for CID of the m/z 414 from the FC-43 cal gas was 150.750 kHz. The waveform was used for a monopolar excitation of the m/z 414. The amplitude of the CID waveform was corrected for monopolar excitation. It was necessary to apply $7.5V_{(0\text{-}p)}$ when only using one end cap at a q_z of 0.4 to achieve the same level of fragmentation as with dipolar CID.

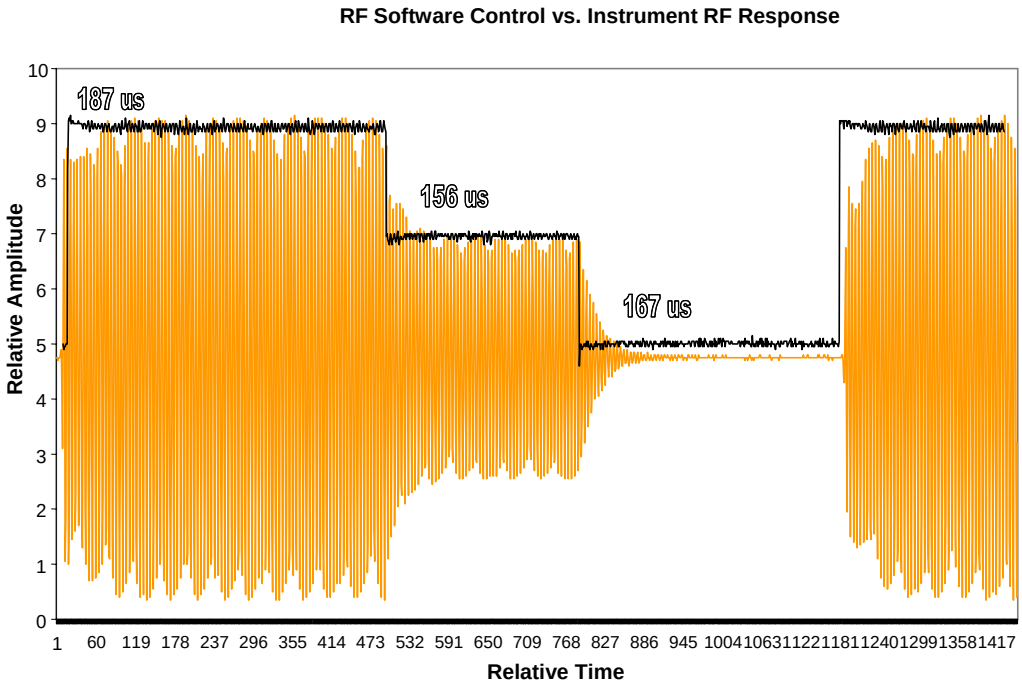

Figure 3.1. Shows the relative lag time between the software control settings of the RF level and the actual instrumental response.

Analysis of the effect of the amplitude of the CID pulse preceding the pulsed q determined that an optimized amplitude existed for each precursor ion studied which corresponds to conventional CID results. There was no noticeable improvement in high amplitude, fast CID efficiency by switching from a dipolar CID excitation to the monopolar setup. While timing was better controlled in the monopolar CID process, the increase in CID amplitude necessary for fragmentation of the precursor decreased the efficiency of the process and negated any advantage of the timing control. The monopolar CID was necessary for the control of timing so that the analysis of the pulse width and also when the delay time between CID and pulsed q could be determined.

The amplitude of the CID pulse was first optimized to determine the most efficient amplitude necessary for formation of product ions while maintaining maximum ion intensity within the trap. CID voltages from 0 - 3.2$V_{(0\text{-}p)}$ were studied to determine the optimal amplitude for fragmentation of the m/z 414 from the FC-43 cal gas at a q_z of 0.4 shown in Figures 3.2 and 3.3. Further exploration of the CID amplitude when combined with the pulsed q method was necessary to achieve efficient fragmentation of the precursor ion. FC-43 cal gas was used because it has distinct fragments at m/z 414, 264, 214, 131, and 69. The m/z 414 was selected as the precursor ion and it fragments to the m/z 69 in the full scan mode. For MS/MS analysis of the m/z 414, the m/z 69 product ion falls below the LMC at a CID occurs at a q_z of 0.4.

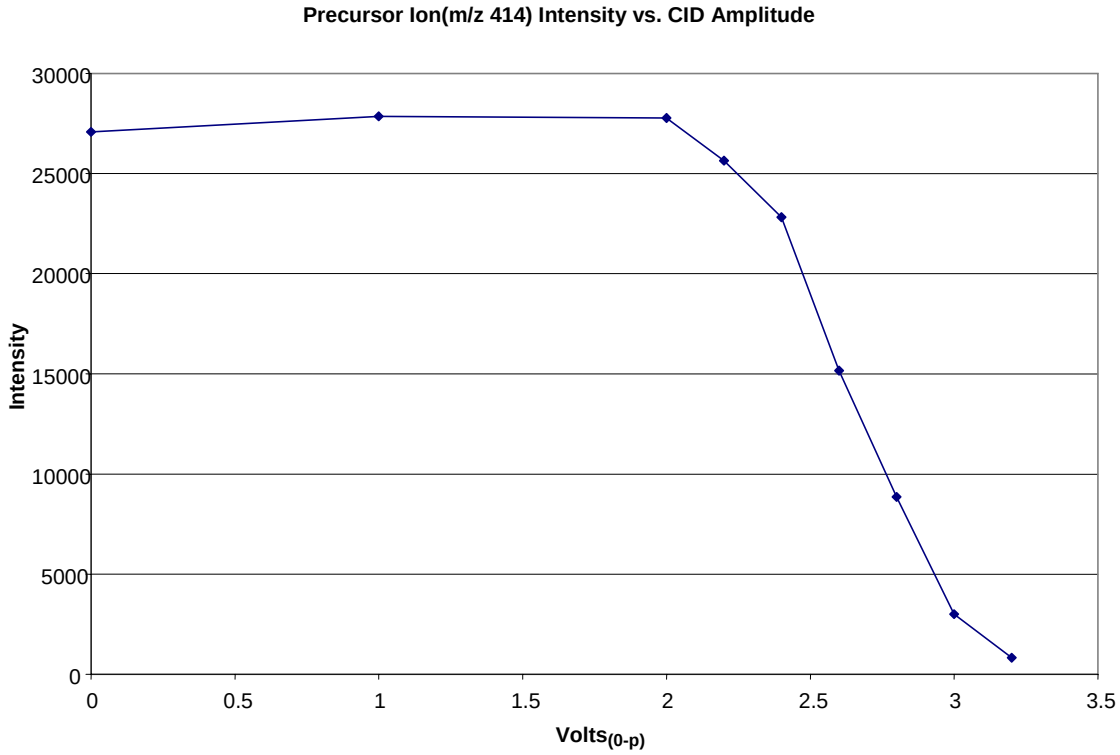

Figure 3.2. Precursor ion intensity of the m/z 414 decreases as the CID amplitude becomes greater than 2$V_{(0\text{-}p)}$, however some precursor is still present at 2.8$V_{(0\text{-}p)}$ before being completely ejected after 3$V_{(0\text{-}p)}$.

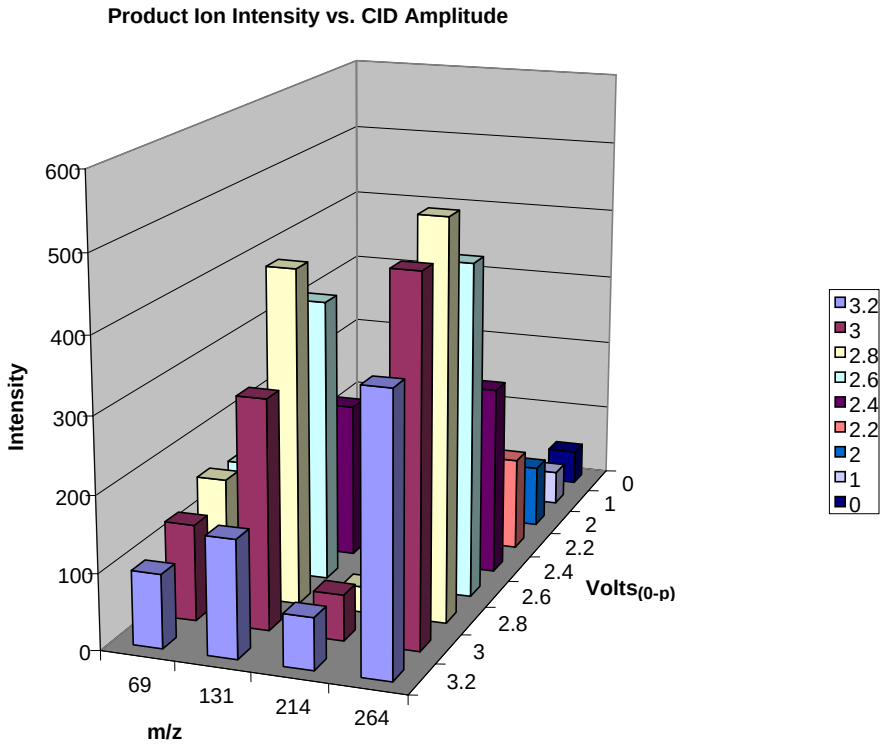

Figure 3.3. Product ion intensity for FC-43 cal gas plotted against CID amplitude with a 100μs pulse width at a q_z level dropped to 0.15. The graph shows that a peak in product ion intensity occurs with a CID amplitude equal to $2.8V_{(0\text{-}p)}$.

An amplitude of $2.8V_{(0\text{-}p)}$ was determined to lead to the most efficient MS/MS results for fragmentation m/z 414. However, in order to further explore the high amplitude, fast CID and its effect on the fragmentation of the ions, it was necessary to switch to the molecular thermometer n-butylbenzene. n-butylbenzene was used to study the internal energy imposed on the m/z 134 molecular ion under the different CID conditions.[23, 27-31] Fragmentation of the m/z 134 molecular ion can occur by two different pathways controlled by the internal energy. The more energetic pathway is that of direct cleavage of a carbon-carbon bond to form the m/z 91 ion(1.7eV). Shown in Figure 4 is the less energetic pathway corresponding to a rearrangement of the molecular ion to form m/z 92 ion(1.1eV).[24, 27, 29, 30, 32] Therefore, the fragmentation pathway can elucidate the relative amount of internal energy forced into the m/z 134 molecular ion during CID.

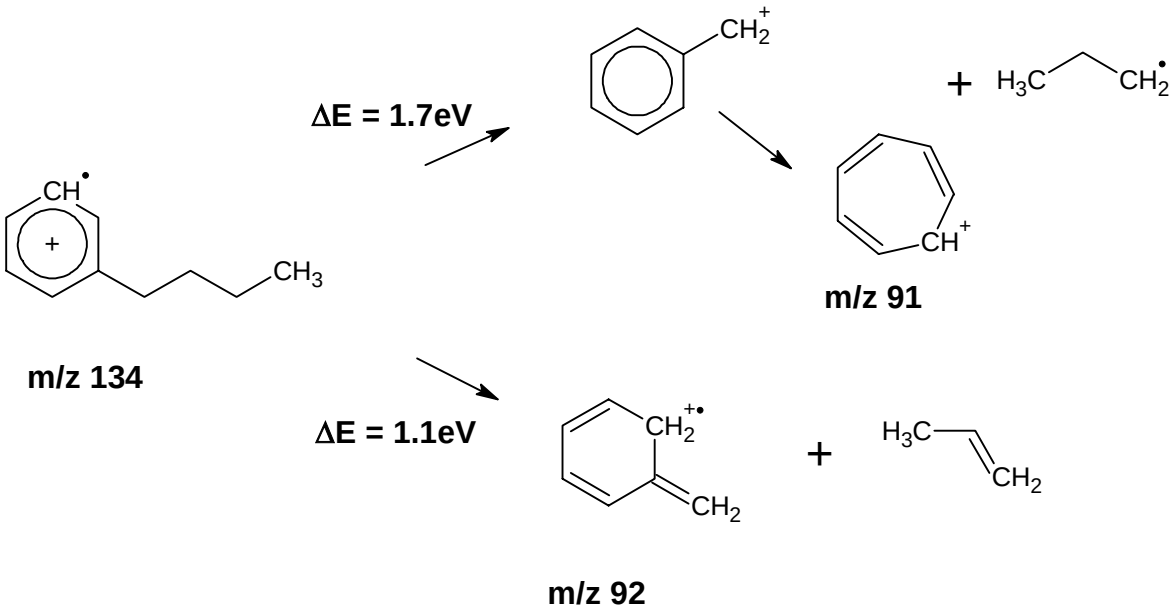

Figure 3.4. Fragmentation of m/z 134 ion.

In conventional CID, the long dipolar CID pulse width, 20 ms, leads to the formation of the m/z 91 upon fragmentation of m/z 134. Preliminary studies using conventional CID showed that an increase in CID amplitude while keeping the pulse width constant increased the ratio of the m/z 91/92. This result is most likely do to, as mentioned previously, more internal energy was imposed on the m/z 134. Further analysis with conventional CID holding the amplitude constant while increasing the pulse width had the same result as increasing the CID amplitude. As the m/z 134 precursor ion had more time to collide with helium, even at a low CID amplitudes($<2V_{(0\text{-}p)}$), the internal energy increased leading to an increase of m/z 91/92.

Study of the effect of a high amplitude, fast CID process was then analyzed so that the energetics of the process could be elucidated. Data collected for the m/z 134 of n-butylbenzene and the determination of the amount of internal energy put into the molecular ion was collected using the monopolar CID method. The monopolar CID differs from conventional CID, but as stated previously had no detrimental effects on the results. From analysis of the m/z 134 ion and its products, it appeared that high amplitude, fast CID caused the total ion intensity to increase as the CID amplitude was increased shown in Figure 3.5. At an amplitude of $1.25V_{(0\text{-}p)}$, there appeared to be a maximum in total ion intensity. Lower amplitude pulses were not sufficient to lead to the

fragmentation of the m/z 134 ion. Higher amplitudes lead to the ejection of both the m/z 134 and the product ions from the trap.

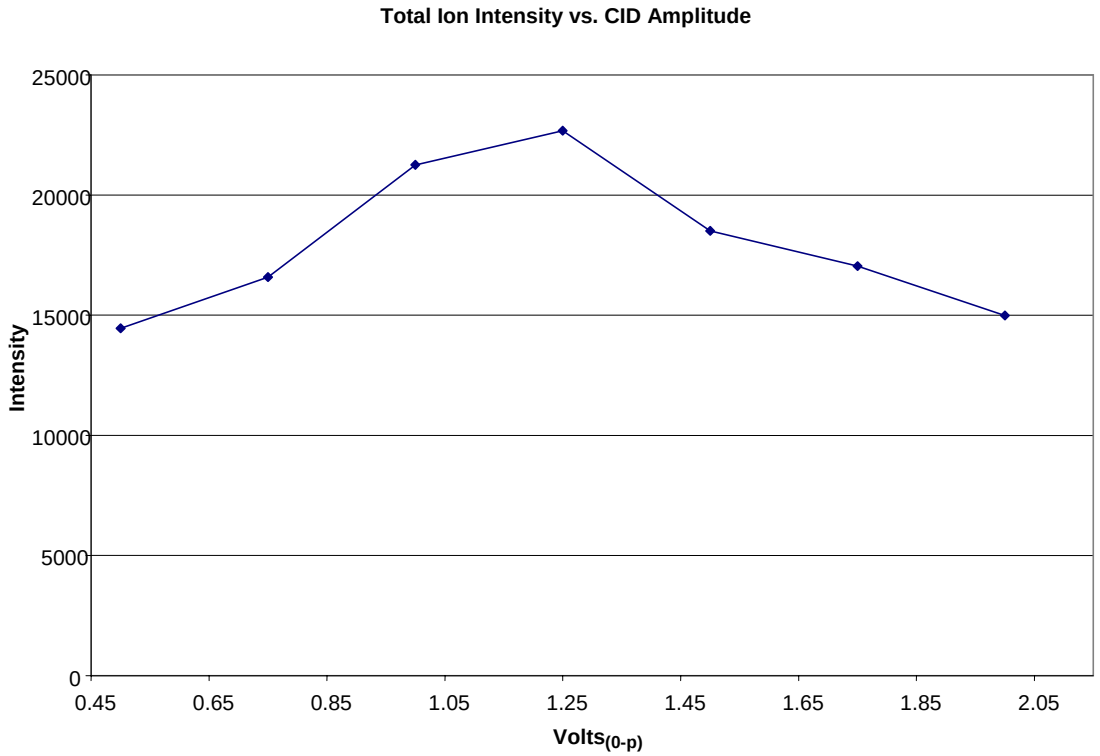

Figure 3.5. Total ion intensity plotted against CID amplitude. There was a slight peak at $1.25V_{(0\text{-}p)}$.

Analyzing the effect of the CID amplitude on the intensity of the m/z 134 ion showed a decrease in intensity with an increase in CID amplitude shown in Figure 3.6. The intensity of the m/z 134 ion approaches zero as the voltage reaches $1.25V_{(0\text{-}p)}$ as at higher amplitudes it is ejected from the trap. Analysis of the intensity of the product ions from m/z 134 showed that the intensity of the m/z 92 appeared to peak at $1V_{(0\text{-}p)}$. The most likely reason for the peak in intensity of the m/z 92 was that the CID pulse was not energetic enough to lead to formation of the m/z 91 from fragmentation of the m/z 134 ion. The intensity of the m/z 91 appeared to peak at $1.25V_{(0\text{-}p)}$. This maximum implies that the energy of the CID pulse was enough to cause the fragmentation of the m/z 134 ion to take the more energetic pathway. The individual ion intensity results showed the effect of amplitude on the CID efficiency. CID efficiency can be defined as the CID amplitude being great enough to cause fragmentation of the precursor ion but not great

enough to eject all ions from the trap. The efficiency of the CID process seems to be greater than 100% at an amplitude of $1.25V_{(0\text{-}p)}$. This result was theoretically impossible. However, the results imply that some sort of optimum CID process occurred when the amplitude was $1.25V_{(0\text{-}p)}$. The results could be slightly skewed by the fact that n-butylbenzene had to be introduced by GC and there was error between injections seen in the large error bars in Figure 3.6. Each data point corresponds to the average intensity of five GC injections.

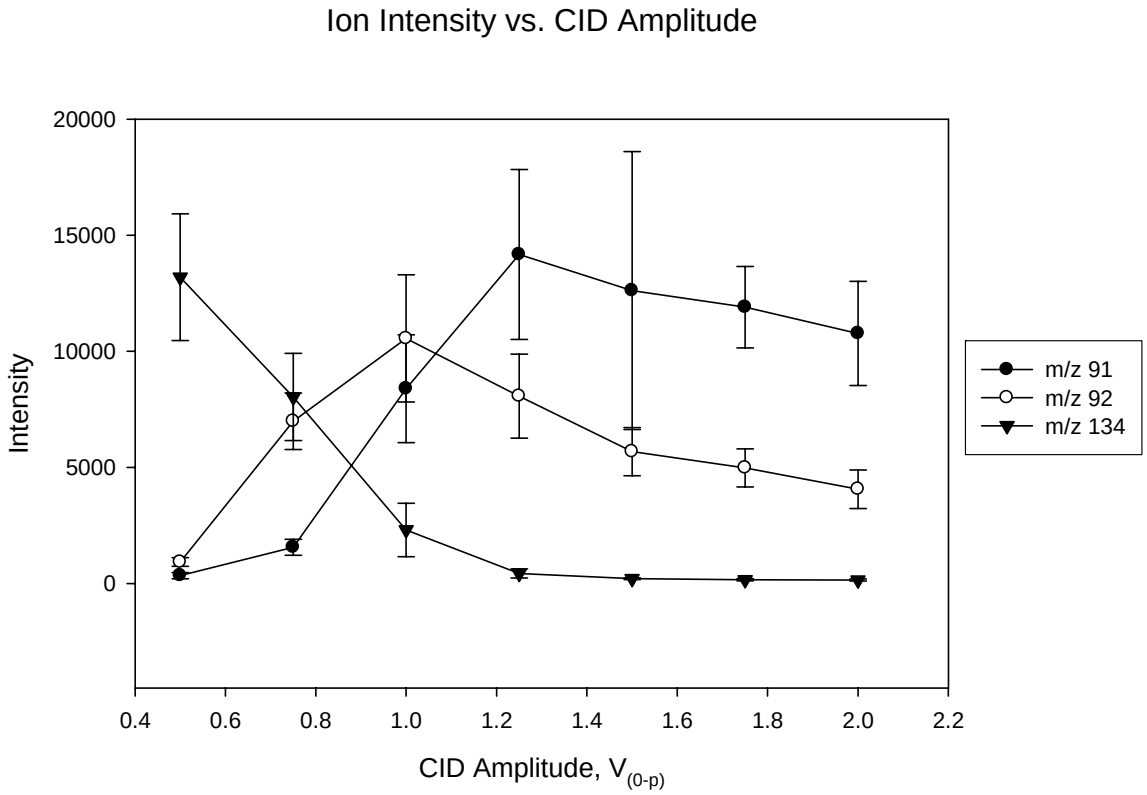

Figure 3.6. Ion intensity(m/z 91, 92, 134) from n-butylbenzene plotted against CID amplitude.

The effect of the CID pulse width was then studied using n-butylbenzene. An increase in CID pulse width, or time allowed for CID, caused results similar to that of the change in CID amplitude. The CID amplitude was set constant to $1.25V_{(0\text{-}p)}$. As the pulse width was increased, the more energetic m/z 91 was formed from fragmentation of the m/z 134. The intensities of the m/z 91, 92, and 134 ions were plotted against the CID pulse width shown in Figure 3.7. A 100 μs pulse lead to the intensity of the m/z 91 being less than the intensity for m/z 92. This result suggested that the area under the curve of

the 1.25$V_{(0\text{-}p)}$ 100 μs CID pulse possessed enough energy to lead to the formation of the m/z 91 ion. The m/z 134 ion had a constant intensity except at 100 μs, where the intensity was an order of magnitude more intense than at any other pulse width. This result showed that once the pulse width was greater than 100 μs, the energy of the CID pulse was sufficient to cause a more efficient fragmentation of the m/z 134.

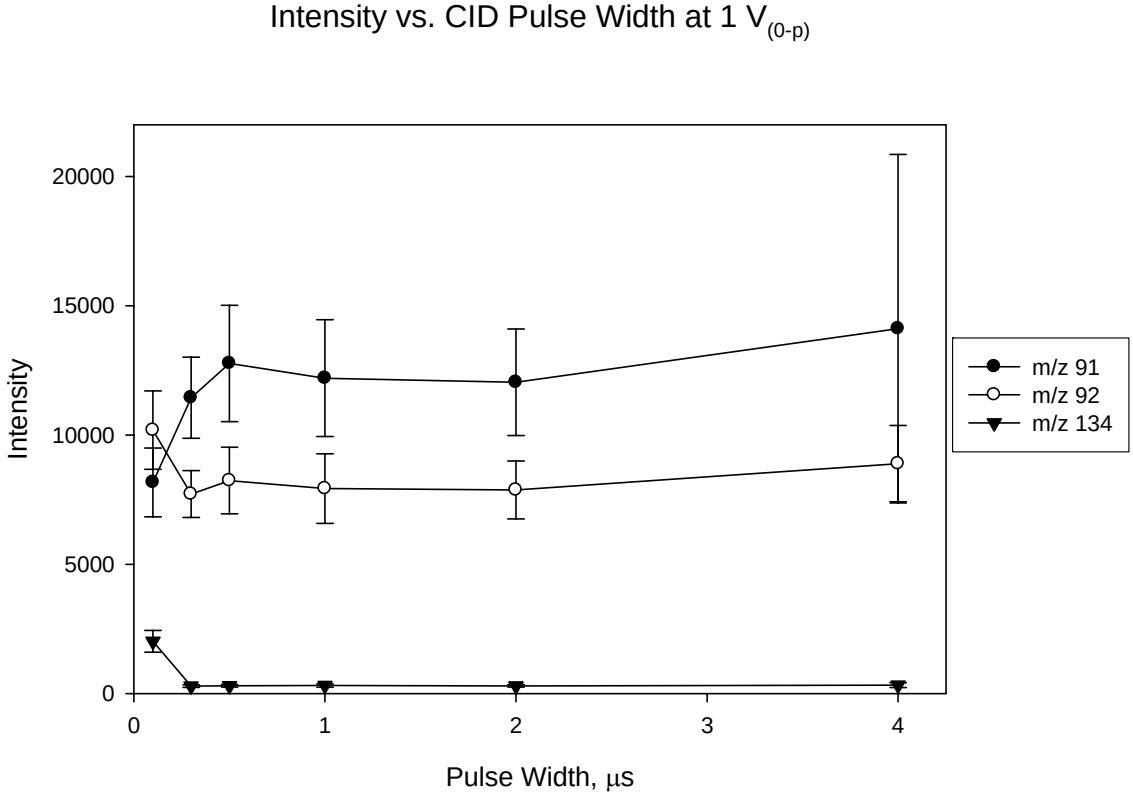

Figure 3.7. Individual ion intensity versus CID pulse width.

After studying the fast, high amplitude CID pulse as a single process, it was combined with a pulsed q experiment. Analysis of the CID process combined with pulsed q allowed for a greater understanding of the combined processes which was the goal of this research. Combined with pulsed q, the amplitude of the CID pulse and its effect on the energy of the m/z 134 of n-butylbenzene was analyzed. The first analysis in this phase of the experiment was analysis of the ratio of m/z 91/92 versus the CID amplitude. The results are shown in Figure 3.8. CID amplitudes less than 1$V_{(0\text{-}p)}$ caused the ratio of m/z 91/92 to be less than unity suggesting a less energetic CID process. The CID amplitude was great enough to lead to ratios of m/z 91/92 greater than unity at CID

amplitudes greater than $1V_{(0\text{-}p)}$. At the higher amplitudes, the ratio becomes increasingly large due to more internal energy being imparted into the m/z 134 ion.

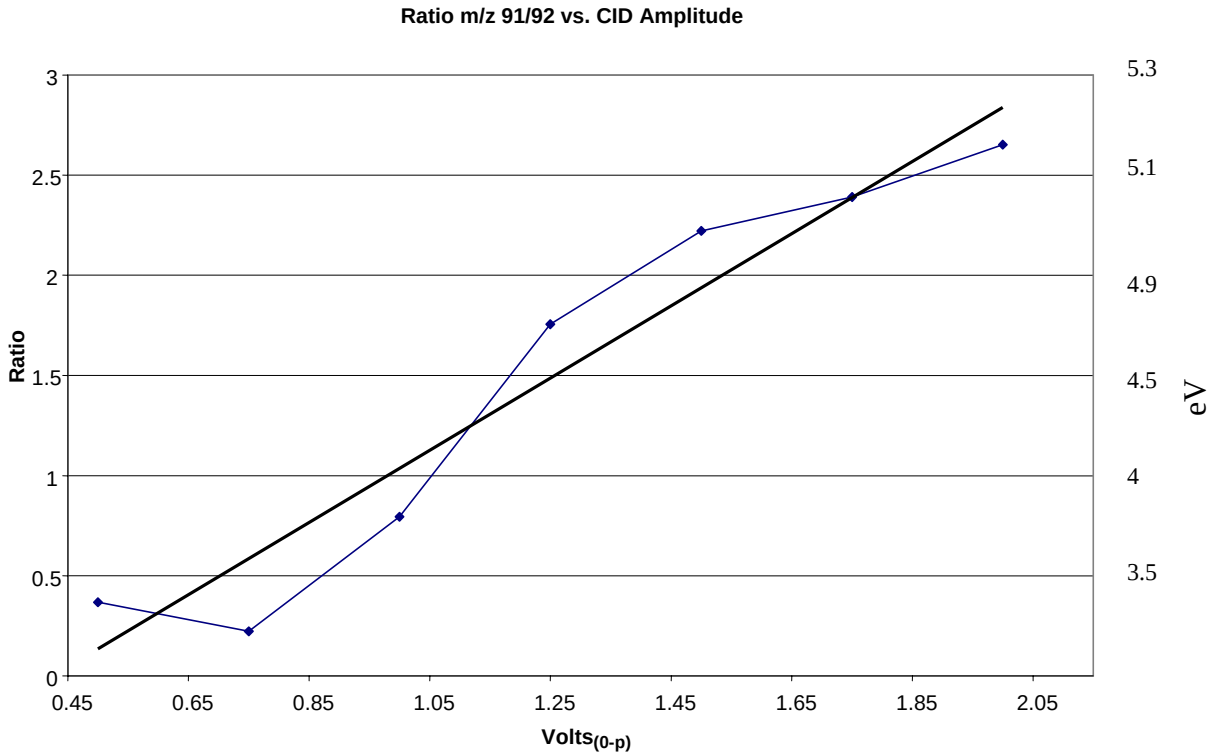

Figure 3.8. Ratio of the m/z 91/92 intensity plotted against CID amplitude and corresponding internal energy.[27]

The effect of the CID pulse width when combined with pulsed q was then analyzed. As shown in Figure 3.9, the effect of the CID pulse width had similar results as the previous study on the effect of the CID amplitude. The results clearly show that the ratio of m/z 91/92 was only less than unity when the pulse width was less than 500 μs. As the pulse width increased, the amount of internal energy of the m/z 134 ion increased during the CID process.

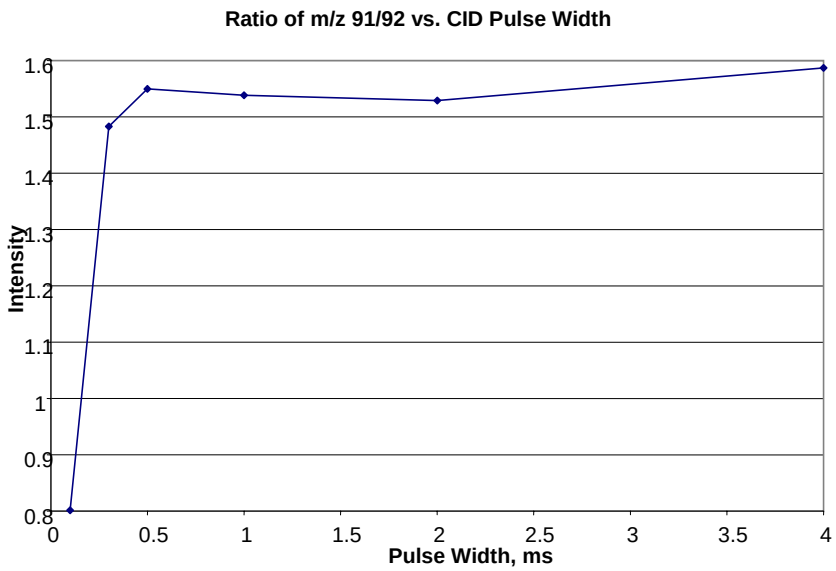

Figure 3.9. Ratio of the m/z 91/92 intensity plotted against CID pulse width.

Determination of the effect of the CID pulse width and amplitude elucidated the differences in energy between the conventional CID process and the high amplitude, fast CID process. From the empirical results, it appeared that the high amplitude, fast CID process was a very energetic CID process as was seen by the ratio of the m/z 91/92 ions from n-butylbenzene. The result that lead to the conclusion that the pulsed q method incorporated a higher energy CID process contributed to the conclusion that the dropping of the q_z level itself imposed some kinetic energy into the ion. From previous studies, the ratio of the m/z 91/92 ions can be directly correlated to the energy of the CID pulse. From the graph of this relationship published elsewhere,[27] but shown in Figure 3.8, it appeared that the energy of the CID pulse was approximately 4.5eV when the CID pulse was 100μs wide and 1.25$V_{(0\text{-}p)}$ in amplitude.

The effect of the time at which the CID pulse was invoked versus when the q_z level was lowered was studied. The DDG was used to set the delay time between the two events the DDG. A 100 μs wide CID pulse was used. The results for the m/z 414 ion from the FC-43 cal gas in Figures 3.10-3.12 showed when the CID process was most efficient. The efficiency was measured by the intensity of the m/z 69 ion shown in Figure 3.11. The intensity of the m/z 69 had the greatest intensity when there was a very short time, ~300 μs, between when the CID pulse was applied and the q_z was lowered. Once the CID pulse overlapped the point at which the q_z began to drop, the ion count

decreased to near zero suggesting that all the ions were being ejected from the trap, which was due to the CID now taking place at a q_z of 0.1 for the m/z 414 ion.

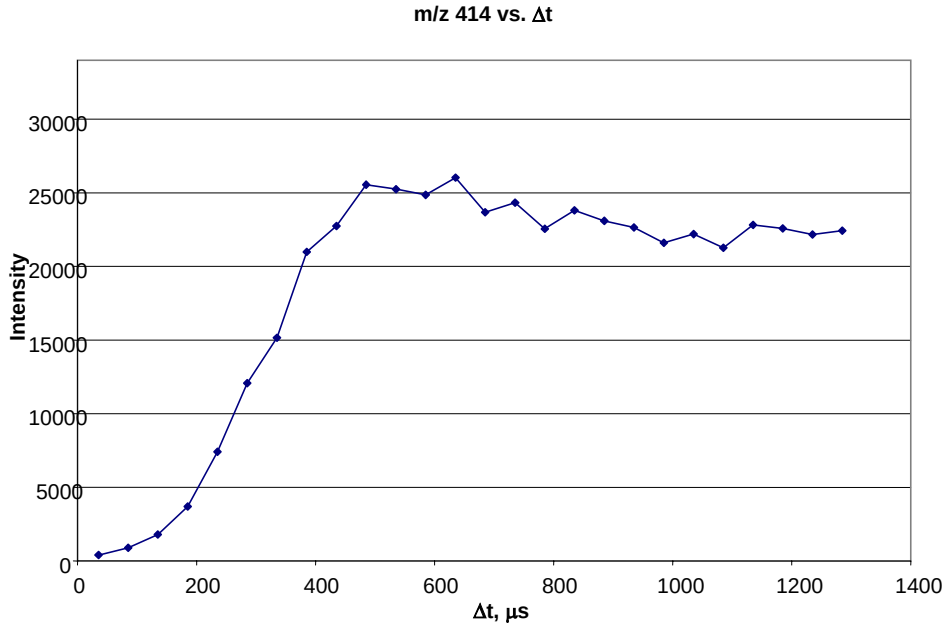

Figure 3.10. Intensity of the m/z 414 precursor ion plotted against time between CID $2.8V_{(0\text{-}p)}$ pulse and the dropping of the q_z level.

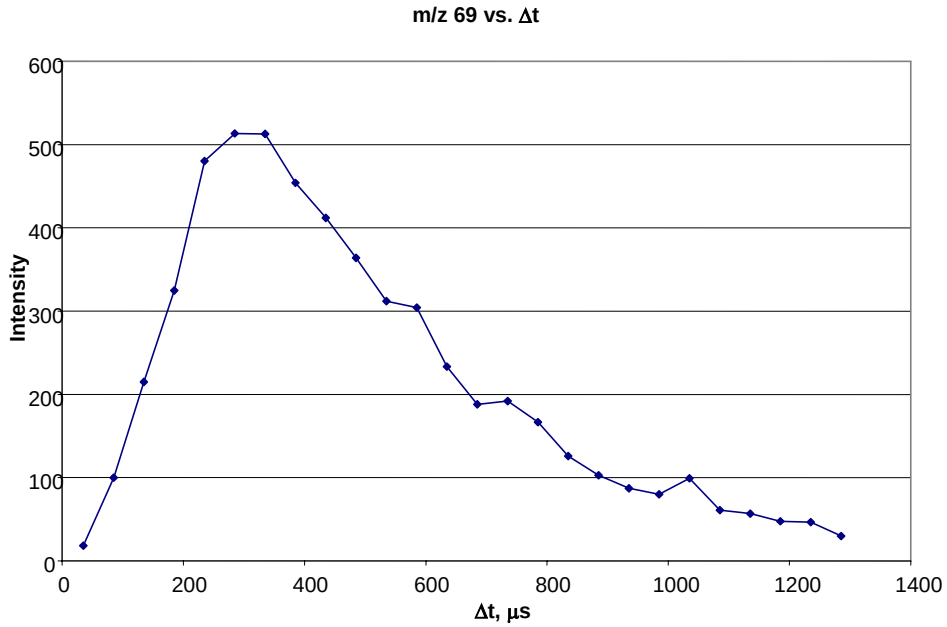

Figure 3.11. Intensity of m/z 69 plotted against time between the end of the CID pulse and the dropping of the q_z level.

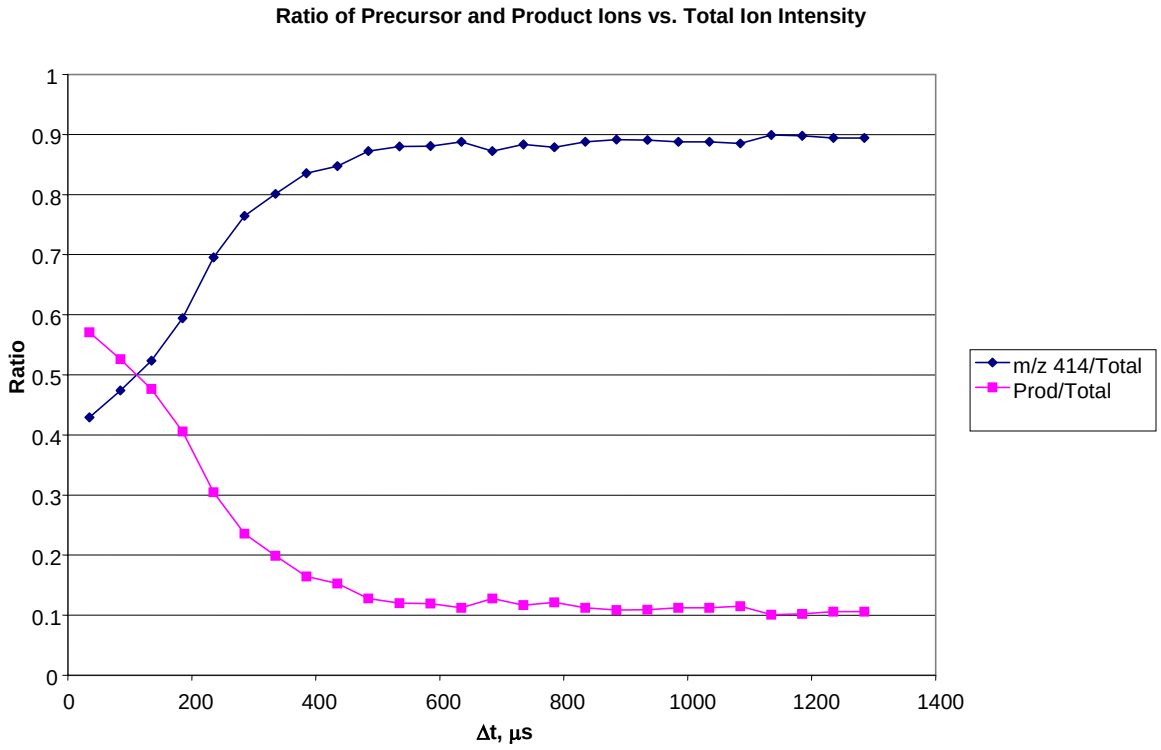

Figure 3.12. The ratio of the intensity of the m/z 414 precursor ion and product ions(m/z 69, 131, 214, 264) to the total ion intensity plotted against time between the end of the CID 2.8$V_{(0\text{-}p)}$ pulse and the dropping of the q_z level.

The effect of the CID pulse width in combination with the pulsed q method was further studied. The CID pulse started at 50 μs before the q_z level was lowered, and then increased from that point. The time interval between the end of the CID pulse and the lowering of the q_z level was held constant at 50 μs. The pulse width was increased by 10 μs until a width of 160 μs. At 160 μs, the ion intensity approached zero as the ions were ejected from trap due to the increase in pulse width. Increase in the pulse width beyond 160 μs created a more energetic CID pulse. The ion intensity of the m/z 414 began to decline as the pulse width became greater than 90 μs shown in Figure 3.13. At a pulse width of 100 μs, the intensity of the m/z 69 was at a maximum as shown in Figure 3.14.

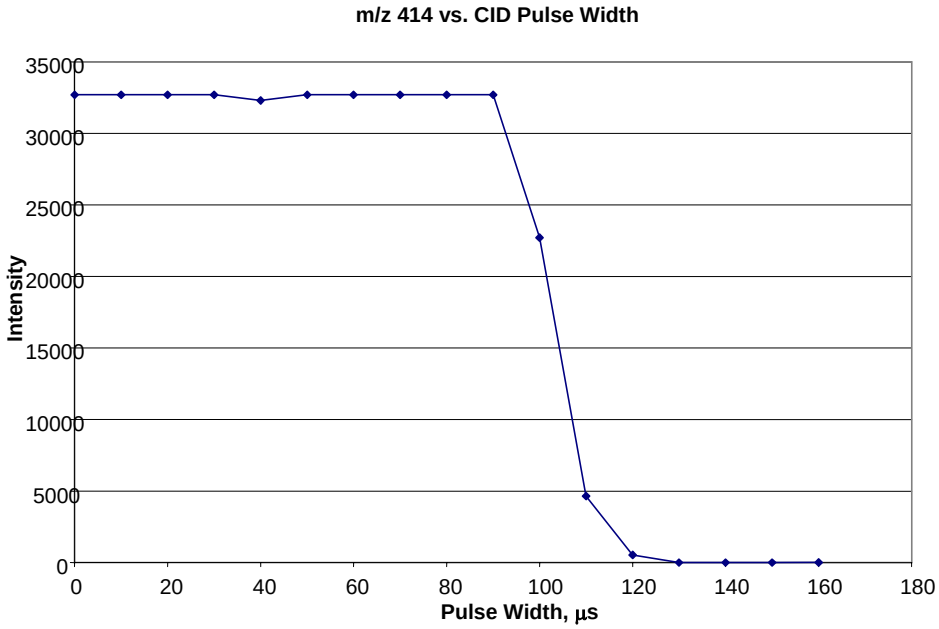

Figure 3.13. Intensity of the m/z 414 precursor ion plotted against the CID pulse width at $1V_{(0\text{-}p)}$.

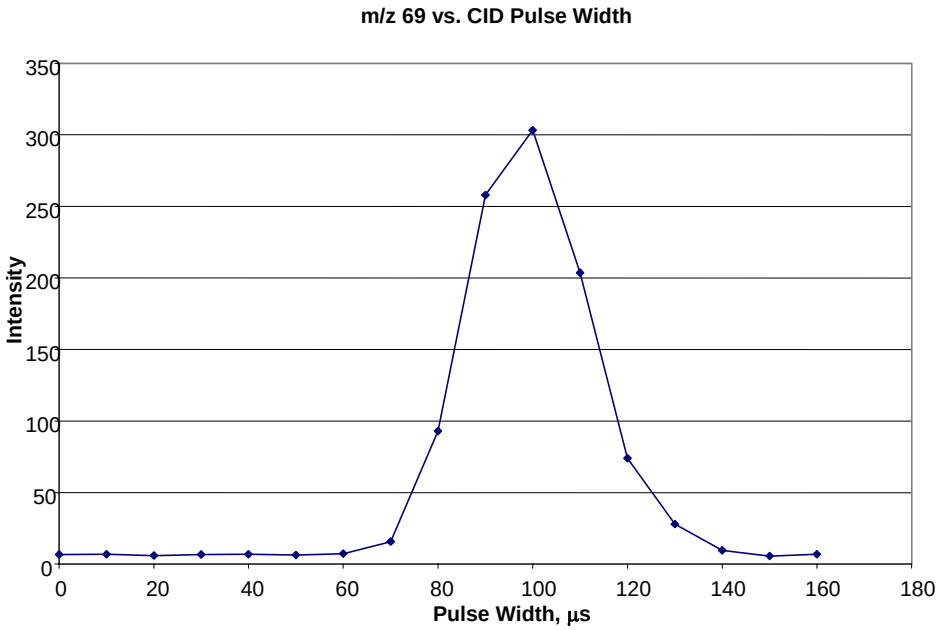

Figure 3.14. Intensity of the m/z 69 ion from the m/z 414 ion of the FC-43 cal gas plotted against CID pulse width at $2.8V_{(0\text{-}p)}$.

At pulse widths lower than 70 µs, the energy was not great enough for sufficient fragmentation of the m/z 414 ion, while pulse widths greater than 130 µs have sufficient energy to eject all the ions from the trap. As the pulse width becomes longer than 70 µs,

the ratio of the product ions to total ion intensity approaches unity. Once the pulse width becomes 130 μs wide, all ions are ejected from the trap. It was determined that a pulse width of 100 μs causes enough fragmentation of the precursor m/z 414 ion, while not ejecting the m/z 69 product ion from the trap.

At the same CID pulse widths the ratio of the m/z 414 precursor ion to total ion intensity decreases to near zero. The ratio of the m/z 414 and the product ions to the total ion intensity gave more insight into the effect of the CID pulse width on the results shown in Figure 3.15. From the figure, the product ion ratio began to increase and the m/z 414 ratio began to decrease at a width greater than 80 μs.

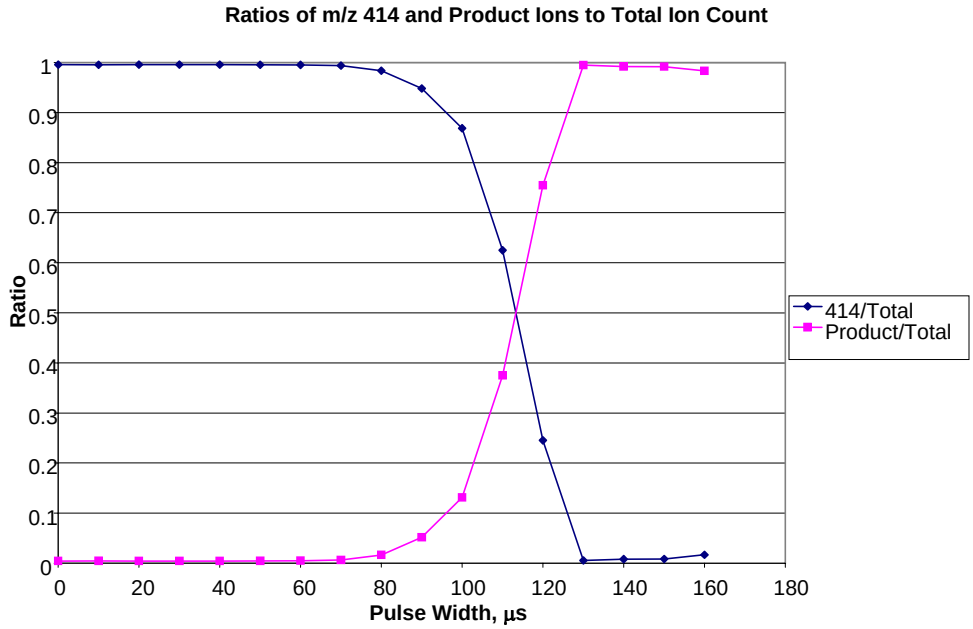

Figure 3.15. Ratios of m/z 414m/z precursor and product ions intensity plotted against CID pulse width.

Pulse widths greater than 115 μs result in the m/z 264 ion being most abundant. This result was important as the m/z 264 ion factored into the total ion intensity. The ratio of m/z 69 to the total ion intensity results in a peak at 120 μs shown in Figure 3.16. Complete fragmentation of the m/z 414 occurred when the pulse width reached 130 μs and ejection of the m/z 414 ion began to occur at pulse widths greater than that. The results of the effect of the combined processes on the ratio of product and precursor ions from the FC-43 cal gas are slightly skewed from results on the ion intensity alone. The

difference in the pulse width where the CID process appeared the most efficient occurred because the total ion intensity is slightly decreased at a 120 μs CID pulse width. The decrease in intensity was due to the near 100% fragmentation of the m/z 414 and the production of m/z 264 and m/z 69.

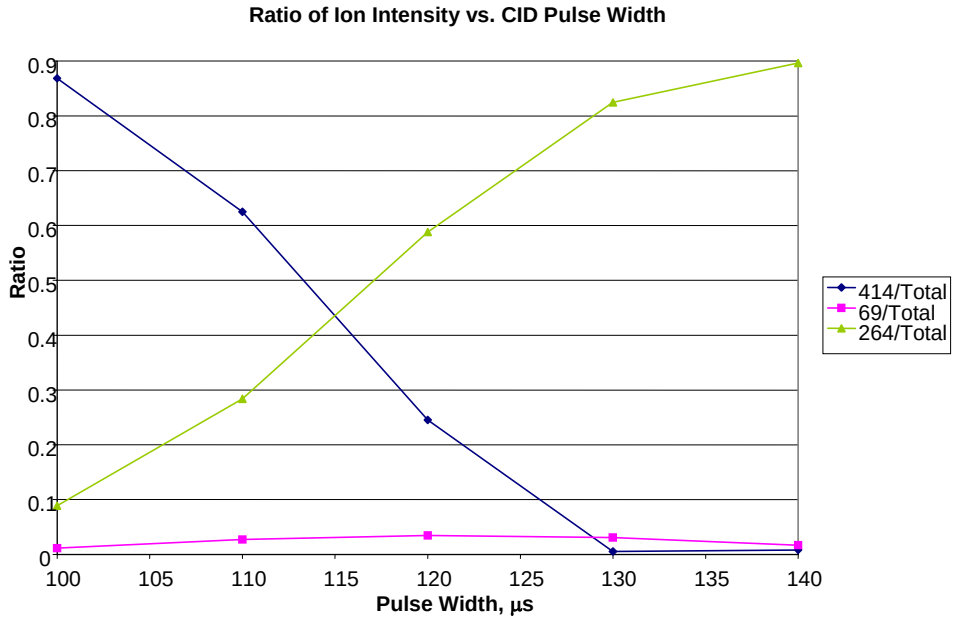

Figure 3.16. Ratios of the m/z 414, 69, 264 to the total ion count was plotted against CID pulse width.

Results of the properties of lowering the q were then studied. The q_z level that the RF amplitude was lowered to appeared to have an impact on the intensity of the product m/z 69 shown in Figure 3.17. From the figure, there appeared to be a peak in intensity when the q_z level was lowered from 0.4 to 0.11. The results show that the optimal q_z level to lower to should be 0.11. When the q_z level was lowered below 0.11, it became harder to store both the precursor and product ions from the m/z 414 ion within the QIT. When the q_z level was lowered from 0.4 to any level above 0.11, the effect of the LMC became apparent as low m/z ions were no longer seen in the spectra.

In terms of the total ion intensity, there appeared to be a maximum in intensity when the q_z level was lowered from 0.4 to 0.15 shown in Figure 3.18. The total ion intensity was most likely highest because of the presence of some of the m/z 414 ion still being present while sufficient CID fragmentation began to occur. The intensity of the m/z 131 and m/z 264 product ions also peaked when the q_z level was lowered from 0.4 to

0.15. The intensity of the m/z 69 ion was zero until the q was lowered from 0.4 to 0.14 due to the LMC as shown in Figure 3.19.

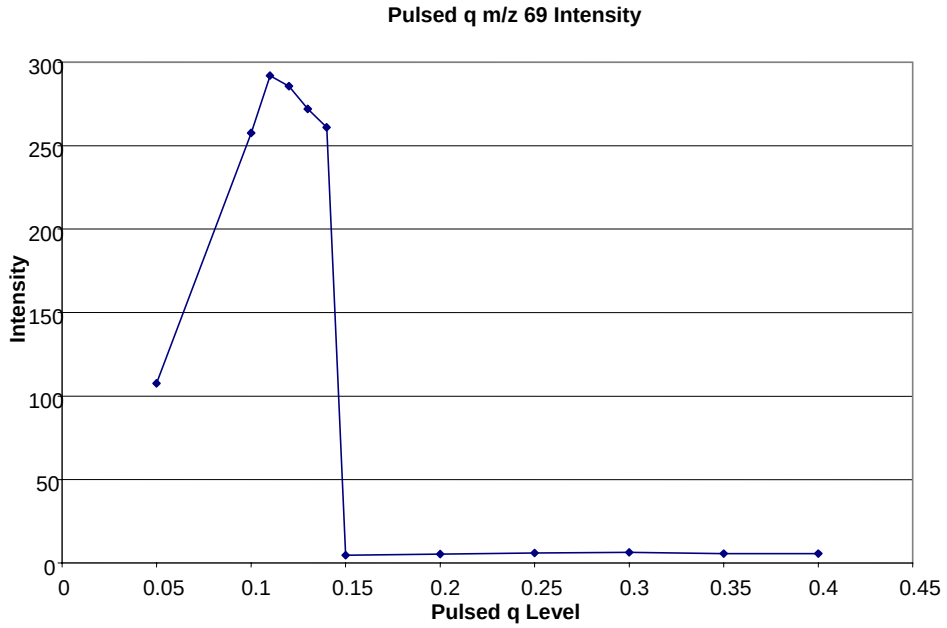

Figure 3.17. m/z 69 intensity plotted against the q_z level the RF was lowered to during pulsed q.

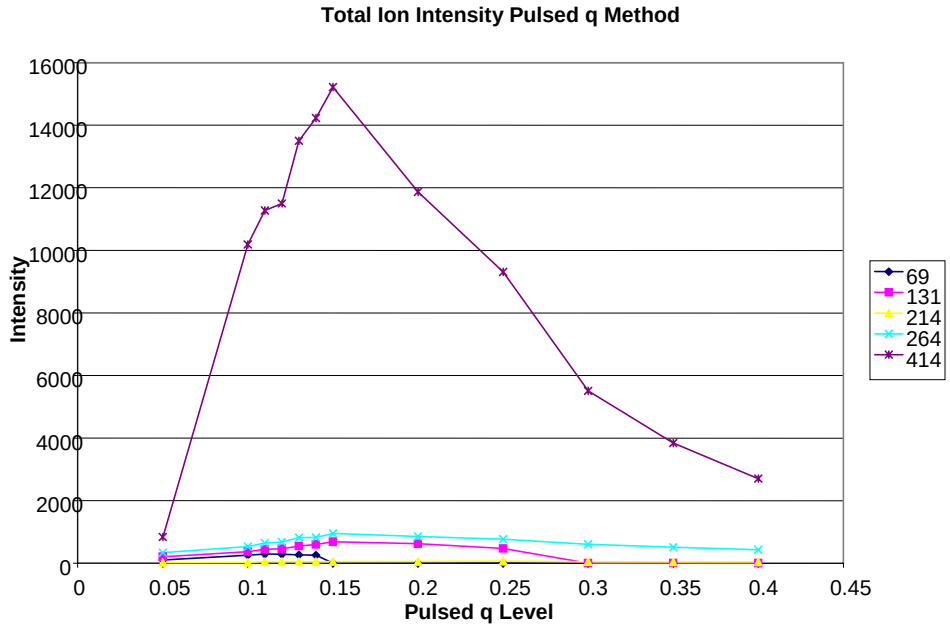

Figure 3.18. Total ion intensity for the pulsed q experiment plotted against the q_z level in which the RF amplitude was lowered exhibits a peak at a q_z of 0.15.

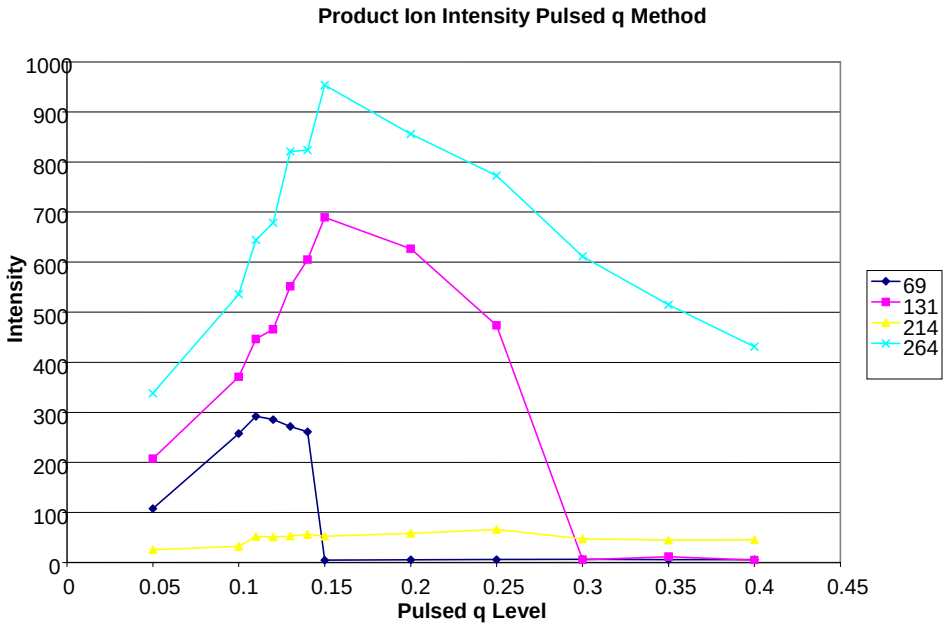

Figure 3.19. Product ion intensity from m/z 69, 131, 214, and 264 ions from m/z 414 of FC-43 cal gas plotted against q_z level the RF amplitude was lowered to during pulsed q.

The energy generated by the q_z level drop alone cannot be enough to lead to fragmentation of the precursor. Therefore, it was necessary to have the fast low amplitude CID pulse fire within 100 μs of the q_z drop. At high enough amplitudes of the CID pulse, the energy generated by the high amplitude, fast CID process is enough to cause sufficient fragmentation of the selected precursor ions. However, the low mass cut off still exists without the lowering of the q_z level. However, by adjusting the CID amplitude, preferential amounts of internal energy appeared to be imposed on the precursor ion in order to preferentially invoke a certain fragmentation pathway such as that shown with the m/z 134 of n-butylbenzene.

After the optimization of the parameters of high amplitude, fast CID using the pulsed q method was finished, an MS/MS spectrum of the m/z 414 ion from the FC-43 cal gas was obtained. Due to the lowering of the qz level during the pulsed q method the ability to store and detect the m/z 69 ion was possible. This result can be seen in the MS/MS spectrum of the m/z 414 ion shown in Figure 3.20. From this spectrum it was possible to see the benefits of the pulsed q method versus conventional MS/MS analysis.

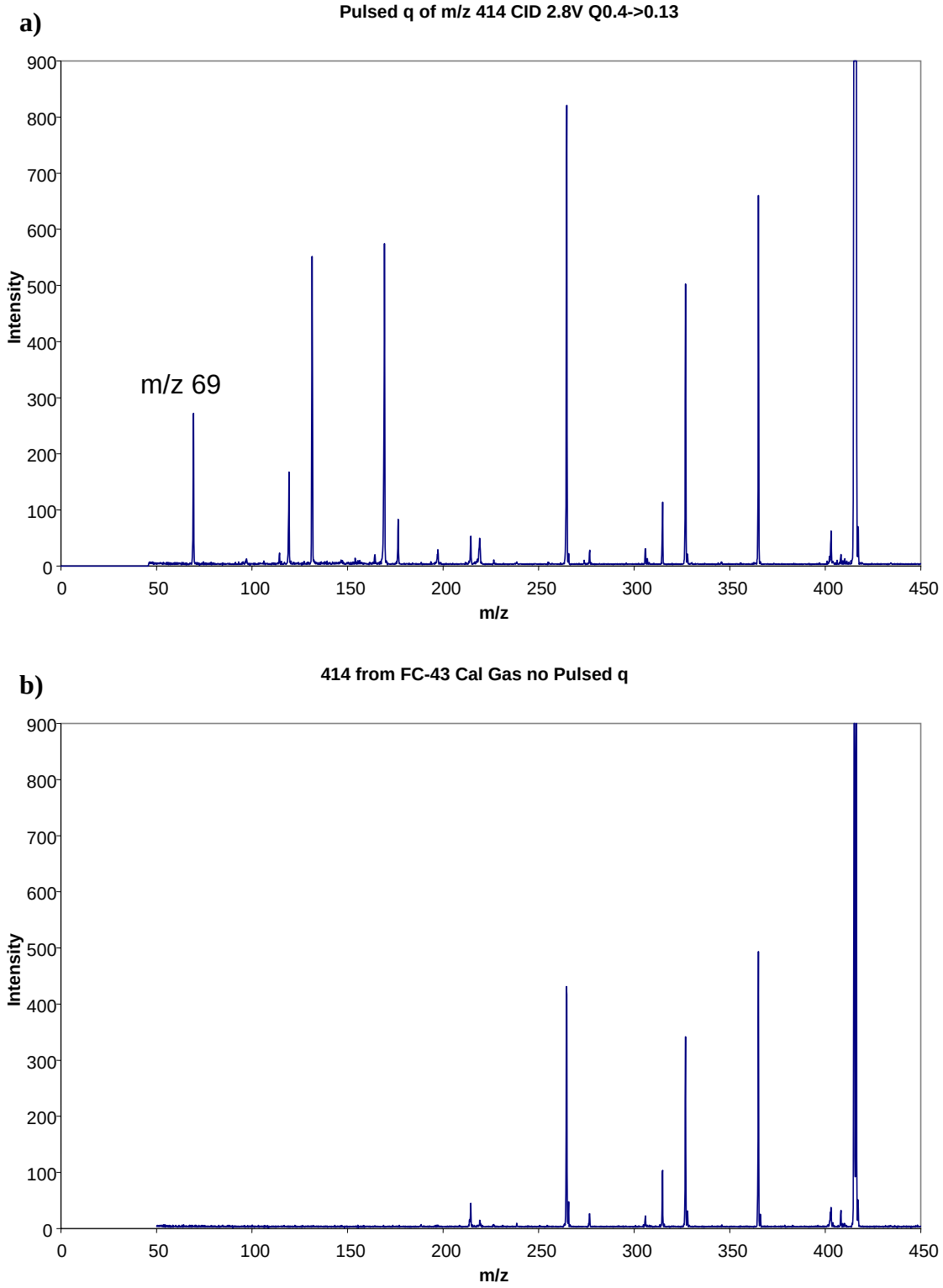

Figure 3.20. a) Optimized parameters for high amplitude, fast CID combined with pulsed q on the FC-43 cal gas occurred when the CID amplitude was $2.8V_{(0\text{-}p)}$ and the q_z was dropped to 0.13. b) MS/MS of the m/z 414 ion with no pulsed q.

Other analytes were studied using high amplitude, fast CID with pulsed q. The m/z 351 of chlorpyrifos which has an m/z 97 product ion that falls below the LMC in MS/MS analysis when the q_z level was 0.4. The appearance of the m/z 97 in the spectrum shown in Figure 3.21 showed the advantage of our technique over conventional CID. The optimized parameters for analysis of the m/z 351 were a CID amplitude of $2.2V_{(0\text{-}p)}$ and the q_z level being lowered from 0.4 to 0.15. In a conventional MS/MS spectrum, the m/z 97 ion would not appear, so the advantage of using our technique can be seen in the spectrum in Figure 3.21.

Furthermore, due to the implications the pulsed q technique described by Schwartz has in the field of proteomics,[9] an amino acid was analyzed using the unified technique. The idea of using an amino acid is that of the issue in proteomics of not being able to see individual amino acids during MS/MS analysis due to the low mass cut off. RF/DC isolation of the m/z 232 precursor ion was used. A 100 μs CID pulse with an amplitude of $2V_{(0\text{-}p)}$ was used, followed by a 100 μs delay before the q_z was dropped to 0.1 shown in Figure 3.22. The appearance of the m/z 73 ion in the MS/MS spectrum clearly showed the advantage of using high amplitude, fast CID coupled with the pulsed q method.

In conclusion, high amplitude, fast CID combined with pulsed q proved to be a very effective method for eliminating the problem of the low mass cut-off in MS/MS analyses. The ability to detect the low m/z product ions from several organic compounds proved to be very informative. Using the n-butylbenzene allowed for the elucidation of the energy of the CID process. Furthermore, the combined technique will prove to be a useful analytical method for the analysis of peptides in proteomics.

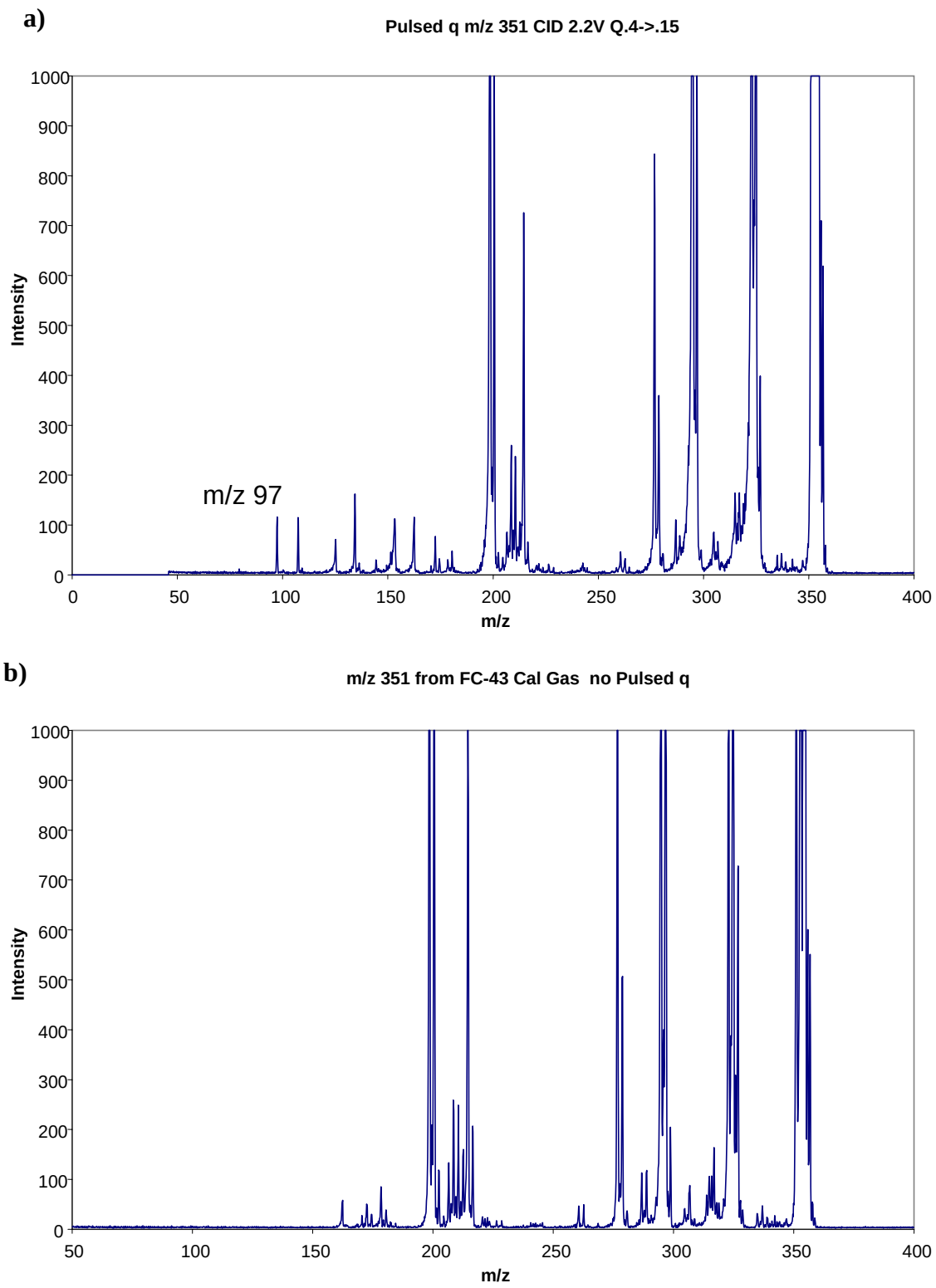

Figure 3.21. a) m/z 97 intensity from m/z 351 precursor ion from chlorpyrifos plotted against m/z. b) MS/MS of the m/z 351 ion without using pulsed q.

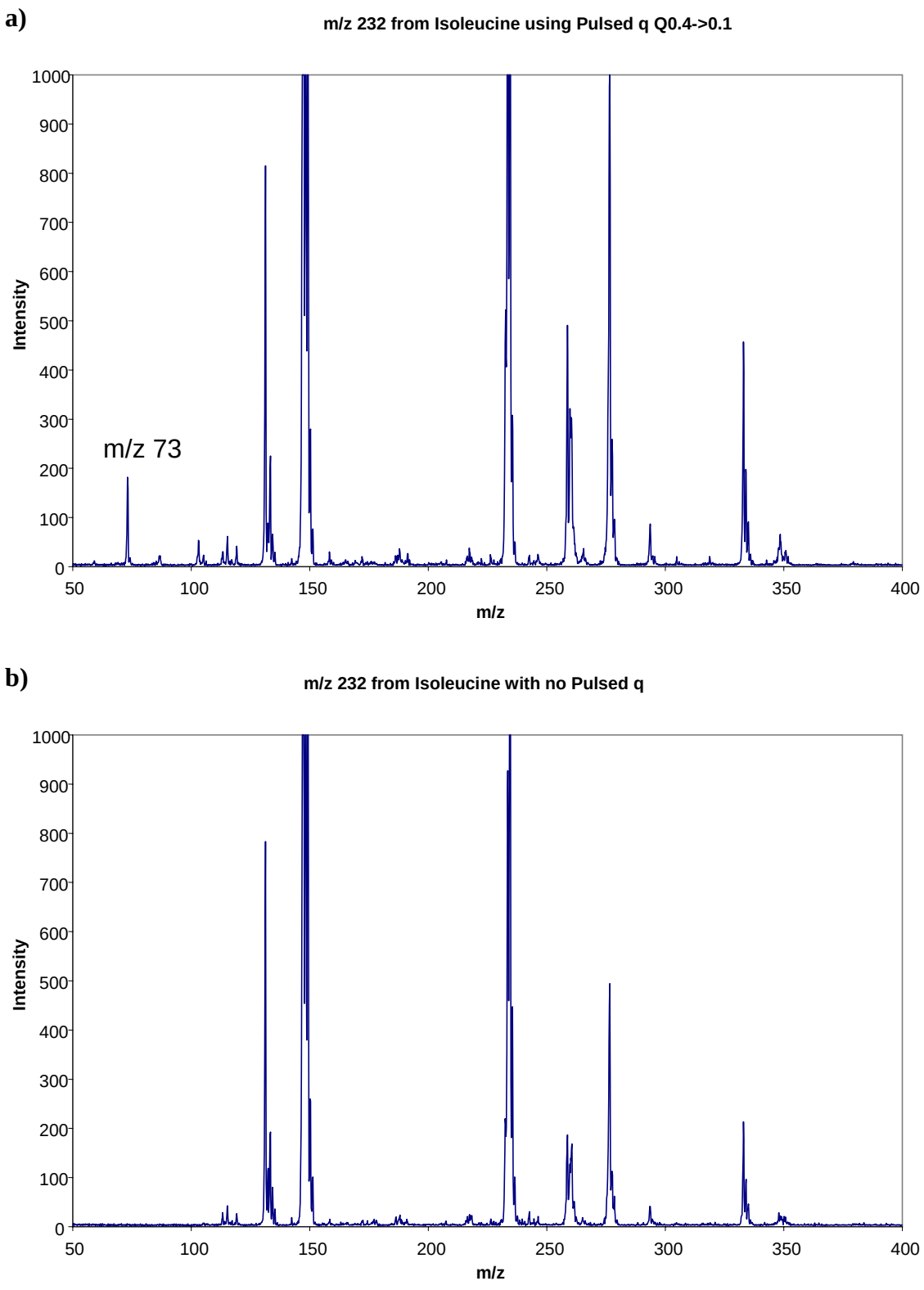

Figure 3.22. a) MS/MS spectrum with pulsed q of m/z 232 from Isoleucine. b) MS/MS spectrum of the m/z 232 ion with no pulsed q.

CHAPTER 4

Conclusion

Mass spectrometry is a useful tool for gaining information about the composition of a compound. MS/MS analysis is an excellent technique to analyze the fragmentation pathways of specific ions. The ability to isolate a specific ion prior to mass analysis so that further analysis of the specific ion can occur is quite useful for understanding the molecular composition of the analyte. Furthermore, collision induced dissociation in MS/MS analysis is a very efficient technique for increasing the internal energy of the ion in order to cause fragmentation. The unique ability to analyze the energy deposition during the CID process through the use of a molecular thermometer reveals the power of MS/MS analysis and the usefulness of the DC tomography and high amplitude, fast CID with pulsed q.

Where an ion is within the trap plays an important role in whether or not the ion will be detected. The location of the ions within the trap also elucidated the property of how much kinetic energy an ion has at a given time. DC tomography allowed for the tracking of the trajectory of the ion motion of the xylene isomers without modification to the ion trap. The study of the ion trajectory could be used to potentially separate molecular ions from isomeric compounds based on the collisional cross section of each ion. Tomography experiments are useful in gaining information on what effect the pressure of the helium has on the motion of the ion. The effect of the trap temperature on the motion of the ion can also be studied by the ion tomography experiments. Ion tomography experiments are most useful in determining the effects of the collisional cross sections of different ions on the mobility of the ion.

The pulsed q method is quite novel in being successful at eliminating the low mass cut off problem in MS/MS analysis. The elimination of the low mass cut off in MS/MS analysis is vital in the area of proteomics. In the case of peptide sequencing from MS/MS spectra, y_1, b_1 and immonium ions are often not detected because they fall below the low mass cut off.[11] The pulsed q method has the ability to detect the m/z 73 product ion from the m/z 232 selected precursor ion of the derivatized isoleucine by dropping the storage q_z level from 0.4 during the CID process to 0.2 immediately after

CID but before the mass selective instability scan. The detection of immonium ions is very important because each immonium ion corresponds to one amino acid that is present in a peptide.[11]

Determination of the effect of the CID pulse width and amplitude elucidated the differences in energy between the conventional CID process and the pulsed q method. From the empirical results, it appears that the high amplitude, fast CID process combined with the pulsed q method was a much less energetic CID process as was seen by the ratio of the m/z 91/92 ions from n-butylbenzene. The results that lead to the conclusion that the pulsed q method incorporated a lower energy CID process contributed to the conclusion that the dropping of the q_z level itself imposes some kinetic energy into the ion. Analysis of the effect of the amplitude of the CID pulse preceding the pulsed q determined that an optimum amplitude exists for each precursor ion studied as was the case for the m/z 134 of n-butylbenzene.

There was no noticeable improvement in CID efficiency by switching from a dipolar CID excitation to the monopolar setup. While timing was better controlled in the monopolar CID process, the increase in CID amplitude necessary for fragmentation of the precursor decreased the efficiency of the process and negated any advantage of the timing control. However, the data collected for the m/z 134 of n-butylbenzene and the determination of the amount of internal energy put into the ion was collected by the monopolar method. The monopolar CID was necessary for the control of timing so that the analysis of the pulse width and also when the delay time between CID and pulsed q could be determined.

The energy generated by the q_z level drop cannot be enough to lead to fragmentation of the precursor ion, therefore it was necessary to have the fast high amplitude CID pulse fire within 100 μs of the q_z drop. At a given amplitude of the CID pulse, the energy generated by the high amplitude, fast CID process is enough to cause sufficient fragmentation without the q_z drop, the low mass cut off still exists. However, by adjusting the CID amplitude, preferential amounts of internal energy appeared to be imposed on the precursor ion in order to preferentially invoke a certain fragmentation pathway such as that shown with the m/z 134 of butylbenzene.

Future Research:

Future research should be directed toward a DC tomography measurement of the motion of the ions during the high amplitude, fast CID process combined with the pulsed q method. It would be interesting to see the effect of the unified process on how the ions move within the trap. Perhaps an even more extensive understanding of the energy process in the high amplitude, fast CID with pulsed q could be gained by the tomography experiment. Perhaps even the effect of the "tickle" pulse during the CID pulse could be studied.

REFERENCES:

1. Skoog, D. A., Holler, F.J., Nieman, T.A., *Principles of Instrumental Analysis*. Harcourt Brace & Company: Philadelphia, 1998.
2. March, R. E., Todd, J.F.J., *Practical Aspects of Ion Trap Mass Spectrometry*. CRC Press, Inc.: Boca Raton, 1995; Vol. 1.
3. March, R. E., An introduction to quadrupole ion trap mass spectrometry. *Journal of Mass Spectrometry* **1997,** 32, (4), 351-369.
4. March, R. E., Quadrupole ion trap mass spectrometry: Theory, simulation, recent developments and applications. *Rapid Communications in Mass Spectrometry* **1998,** 12, (20), 1543-1554.
5. Louris, J. N.; Cooks, R. G.; Syka, J. E. P.; Kelley, P. E.; Stafford, G. C.; Todd, J. F. J., Instrumentation, Applications, and Energy Deposition in Quadrupole Ion-Trap Tandem Mass-Spectrometry. *Analytical Chemistry* **1987,** 59, (13), 1677-1685.
6. Shukla, A. K.; Futrell, J. H., Tandem mass spectrometry: dissociation of ions by collisional activation. *Journal of Mass Spectrometry* **2000,** 35, (9), 1069-1090.
7. Sleno, L.; Volmer, D. A., Ion activation methods for tandem mass spectrometry. *Journal of Mass Spectrometry* **2004,** 39, (10), 1091-1112.
8. Murrell, J.; Despeyroux, D.; Lammert, S. A.; Stephenson, J. L.; Goeringer, D. E., "Fast excitation" CID in a quadrupole ion trap mass spectrometer. *Journal of the American Society for Mass Spectrometry* **2003,** 14, (7), 785-789.
9. Schwartz, J. C., Syka, J.E., Quarmby, S.T. In *Improving the Fundamentals of MSn on 2D Linear Ion Traps: New Ion Activation and Isolation Techniques*, 53rd Annual ASMS Conference, San Antonio TX, 2005; San Antonio TX, 2005.
10. Cunningham, C., Remes, P.M., Burinsky, D.J., Glish, G.L. In *Fast Collision Induced Dissociation for the Identification of Peptides in a Quadrupole Ion Trap Mass Spectrometer*, 53rd Annual ASMS Conference, San Antonio TX, 2005; San Antonio TX, 2005.
11. Kinter, M., Sherman, N.E., *Protein Sequencing and Identification using Tandem Mass Spectrometry.* John Wiley and Sons, Inc.: New York, 2000.
12. Gordon, D. B.; Woods, M. D., Enlarging the Stability Domain for Ion Trap Tandem Mass-Spectrometry (Ms Ms). *Rapid Communications in Mass Spectrometry* **1993,** 7, (3), 215-218.
13. Clemmer, D. E.; Jarrold, M. F., Ion mobility measurements and their applications to clusters and biomolecules. *Journal of Mass Spectrometry* **1997,** 32, (6), 577-592.
14. Creaser, C. S.; Griffiths, J. R.; Bramwell, C. J.; Noreen, S.; Hill, C. A.; Thomas, C. L. P., Ion mobility spectrometry: a review. Part 1. Structural analysis by mobility measurement. *Analyst* **2004,** 129, (11), 984-994.
15. Collins, D. C.; Lee, M. L., Developments in ion mobility spectrometry-mass spectrometry. *Analytical and Bioanalytical Chemistry* **2002,** 372, (1), 66-73.
16. Plass, W. R.; Gill, L. A.; Bui, H. A.; Cooks, R. G., Ion mobility measurement by dc tomography in an rf quadrupole ion trap. *Journal of Physical Chemistry A* **2000,** 104, (21), 5059-5065.
17. Weil, C.; Wells, J. M.; Wollnik, H.; Cooks, R. G., Axial ion motion within the quadrupole ion trap elucidated by dc pulse tomography. *International Journal of Mass Spectrometry* **2000,** 194, (2-3), 225-234.

18. Plass, W. R., Of dipolar dc excitation and dc tomography in the rf quadrupole ion trap. *International Journal of Mass Spectrometry* **2000,** 202, (1-3), 175-197.
19. Wuerker, R. F.; Shelton, H.; Langmuir, R. V., Electrodynamic Containment of Charged Particles. *Journal of Applied Physics* **1959,** 30, (3), 342-349.
20. Knight, R. D.; Prior, M. H., Laser Scanning Measurement of the Density Distribution of Confined Li-6(+) Ions. *Journal of Applied Physics* **1979,** 50, (5), 3044-3049.
21. Lammert, S. A.; Cleven, C. D.; Cooks, R. G., Determination of Ion Frequencies in a Quadrupole Ion-Trap by Using a Fast Direct-Current Pulse as Pump and a Laser Probe. *Journal of the American Society for Mass Spectrometry* **1994,** 5, (1), 29-36.
22. Cleven, C. D.; Nappi, M.; Cooks, R. G.; Garrett, A. W.; Nogar, N. S.; Hemberger, P. H., Selective photodissociation of trapped ions after ion cloud manipulation with an impulsive quadrupolar electric field. *Journal of Physical Chemistry* **1996,** 100, (13), 5205-5209.
23. Lammert, S. A.; Cooks, R. G., Pulsed Axial Activation in the Ion Trap - a New Method for Performing Tandem Mass-Spectroscopy (Ms/Ms). *Rapid Communications in Mass Spectrometry* **1992,** 6, (8), 528-530.
24. Liere, P.; March, R. E.; Blasco, T.; Tabet, J. C., Resonance excitation in a quadrupole ion trap: Modification of competing dissociative channel yields. *International Journal of Mass Spectrometry and Ion Processes* **1996,** 153, (2-3), 101-117.
25. Liere, P.; Blasco, T.; March, R. E.; Tabet, J. C., Influence of Cooling Time on the Internal Energy of Ions Subjected to Resonance Excitation in a Quadrupole Ion-Trap. *Rapid Communications in Mass Spectrometry* **1994,** 8, (12), 953-956.
26. Liere, P.; Bouchonnet, S.; March, R. E.; Tabet, J. C., Cooling time and pressure effects on competitive thermalization activation processes by resonance excitation on ITMS. *Rapid Communications in Mass Spectrometry* **1995,** 9, (15), 1594-1598.
27. Baer, T.; Dutuit, O.; Mestdagh, H.; Rolando, C., Dissociation Dynamics of Normal-Butylbenzene Ions - the Competitive Production of M/Z 91-Fragment and 92-Fragment Ions. *Journal of Physical Chemistry* **1988,** 92, (20), 5674-5679.
28. Goeringer, D. E.; McLuckey, S. A., Evolution of ion internal energy during collisional excitation in the Paul ion trap: A stochastic approach. *Journal of Chemical Physics* **1996,** 104, (6), 2214-2221.
29. Harrison, A. G.; Lin, M. S., Energy-Dependence of the Fragmentation of the Normal-Butylbenzene Molecular Ion. *International Journal of Mass Spectrometry and Ion Processes* **1983,** 51, (2-3), 353-356.
30. Plomley, J. B.; Londry, F. A.; March, R. E., The consecutive fragmentation of n-butylbenzene in a quadrupole ion trap. *Rapid Communications in Mass Spectrometry* **1996,** 10, (2), 200-203.
31. Vekey, K., Internal energy effects in mass spectrometry. *Journal of Mass Spectrometry* **1996,** 31, (5), 445-463.
32. Dunbar, R. C., BIRD (blackbody infrared radiative dissociation): Evolution, principles, and applications. *Mass Spectrometry Reviews* **2004,** 23, (2), 127-158.

VITA

John Edward Spencer
Born: Glendale, West Virginia
Date: March 19, 1981